REVIEW

Check for updates

From metal nitrides to high-entropy nitrides: advances in spectrally selective absorber coatings

Qi-Sen Wang,†[a] Xian-Bin Zhao,†[a] Meng Dong,[b] Rui-Bin Zheng,[ac] Rui-Ting Gao,[d] Cheng-Yu He [ID] *[a] and Xiang-Hu Gao [ID] *[ac]

Spectrally selective absorber coatings (SSACs) are critical for efficient photothermal conversion in solar–thermal systems. Traditional metal nitrides have long served as cornerstone materials for these coatings due to their tunable optical properties and high thermal stability, which yield excellent solar absorptance and low infrared emittance. However, as solar–thermal applications push toward more extreme operating conditions, conventional nitrides are reaching inherent limits, particularly in achieving broadband absorption and resisting high-temperature oxidation. In recent years, high-entropy nitrides (HENs) have emerged to address these challenges by incorporating multiple metal cations into a single-phase nitride. This multi-element design affords unprecedented control over optical properties and significantly enhances thermal stability and corrosion resistance. As a result, HEN coatings exhibit broadband solar absorption and exceptional high-temperature durability beyond the reach of traditional binary nitrides. This review charts the progress from classical nitrides to advanced HENs in SSACs. We discuss fundamental photothermal conversion mechanisms, compare fabrication techniques, and highlight performance breakthroughs that illustrate how entropy-engineered nitrides overcome the bottlenecks of conventional systems. Finally, we outline the remaining challenges and future directions, offering a roadmap for the design of next-generation absorber coatings to meet the stringent demands of advanced solar–thermal technologies.

[a]Key Laboratory of Energy Conservation and Energy Storage Materials of Gansu Province, Research Center for Resource Chemistry and Energy Materials, State Key Laboratory of Solid Lubrication, Lanzhou Institute of Chemical Physics, Chinese Academy of Sciences, Lanzhou 730000, China. E-mail: hechengyu@licp.cas.cn; gaoxh@licp.cas.cn

[b]Key Laboratory of High-temperature and High-pressure Materials and Welding, Mechanical Industry, Dongfang Boiler Group Co., Ltd, Zigong 643001, China

[c]Center of Materials Science and Optoelectronics Engineering, University of Chinese Academy of Sciences, Beijing 100049, China

[d]College of Chemistry and Chemical Engineering, Inner Mongolia Key Laboratory of Low Carbon Catalysis, Inner Mongolia University, Hohhot 010021, China

† These authors contributed equally.

Qi-Sen Wang received his B.S. degree from Changchun University of Technology in 2023. He is currently pursuing his M.S. degree through a joint training program between Lanzhou Jiaotong University and the Lanzhou Institute of Chemical Physics, Chinese Academy of Sciences. His research focuses on the design and development of high-entropy ceramic-based spectrally selective absorption coatings for advanced photothermal applications.

Qi-Sen Wang

Xian-Bin Zhao obtained his B.E. degree from Gansu Agricultural University in 2022. He is currently a master's student in the School of Materials Science and Engineering at Lanzhou Jiaotong University. His research interests include the fabrication and performance optimization of high-entropy ceramic-based spectrally selective absorber coatings for solar–thermal energy conversion.

Xian-Bin Zhao

Broader context

The urgent need for sustainable energy is driving rapid innovation in solar–thermal conversion technologies worldwide. Central to these advances are spectrally selective absorber coatings (SSACs), which serve as the critical interface for converting solar radiation into usable heat while minimizing energy loss. Conventional absorber materials have enabled significant progress but face inherent limitations in durability and efficiency under extreme operating conditions, particularly at high temperatures and in corrosive environments. High-entropy nitrides (HENs), a new class of materials with multiple principal elements, offer an unprecedented combination of broadband solar absorption, exceptional thermal and chemical stability, and robust mechanical properties. These advantages open new horizons for next-generation solar energy systems, including concentrated solar power plants, water purification, and thermal management applications. This review provides a comprehensive synthesis of the mechanisms, fabrication methods, and design strategies underlying both classical and high-entropy nitride coatings. By illuminating the scientific and technological advances in this field, our work highlights the transformative potential of HEN-based SSACs to address pressing global challenges in energy sustainability and to inspire further innovation at the intersection of materials science and solar energy harvesting.

1   Introduction

Solar–thermal technologies have become a prominent focus of renewable energy research due to the growing need for sustainable and efficient energy solutions.[1–5] At the heart of these technologies is photothermal conversion, which refers to the process of capturing sunlight and converting it into heat for use in power generation, desalination, de-icing, and others.[6,7] Spectrally selective absorber coatings (SSACs) are indispensable in this context, as they are engineered to absorb the broad solar spectrum (0.3–2.5 μm) while minimizing thermal emission in the infrared region (2.5–25 μm).[8–11] For decades, transition metal nitrides such as TiN, ZrN, and TaN have been regarded as benchmark materials for SSACs.[9,12] These nitrides offer a unique combination of metallic conductivity, plasmonic behavior, high melting point, and chemical inertness, which enable outstanding solar absorption and durability at elevated temperatures. Moreover, their optical properties can be tuned by adjusting the composition and exploiting intrinsic defect chemistry, allowing the design of coatings optimized for applications ranging from low-to high-temperature regimes.[13]

As solar–thermal systems are deployed in increasingly demanding environments, such as concentrated solar power (CSP) plants and advanced heat management systems, SSACs must deliver not only high spectral selectivity and efficiency but also exceptional thermal stability, oxidation resistance, and mechanical robustness during prolonged exposure to extreme temperatures and corrosive atmospheres.[14–16] Conventional nitrides eventually encounter limitations under these conditions. For example, at ultra-high temperatures, they become prone to oxidation, and their binary composition restricts how much one can tailor their optical response or phase stability. These issues have become critical bottlenecks for further

Rui-Bin Zheng received his B.S. degree from Lanzhou Jiaotong University in 2023 and is currently a PhD candidate at the School of Chemistry and Chemical Engineering, Inner Mongolia University. His research is centered on the development of high-entropy hydrogen storage materials with enhanced thermodynamic stability and kinetics for efficient energy storage.

Rui-Bin Zheng

Cheng-Yu He is a Research Associate Professor at the Key Laboratory of Energy Conservation and Energy Storage Materials of Gansu Province, Lanzhou Institute of Chemical Physics, Chinese Academy of Sciences. He obtained his PhD degree from Lanzhou University of Technology. His research focuses on functional high-entropy materials, with an emphasis on enhancing photothermal performance, regulating heat transfer mechanisms, and exploring their applications in energy conversion and thermal management technologies.

Cheng-Yu He

Xiang-Hu Gao received his PhD degree from the University of Chinese Academy of Sciences. He is currently a Research Professor at the Lanzhou Institute of Chemical Physics, Chinese Academy of Sciences. His research focuses on nanomaterials for energy conversion, with expertise in high-temperature photothermal materials, infrared radiation coatings, and radiative cooling technologies. By integrating theory and practice, he is dedicated to advancing cutting-edge materials for solar energy utilization efficiency and thermal management, addressing global energy challenges while making significant contributions to meeting human needs.

Xiang-Hu Gao

performance improvements and long-term reliability of traditional SSACs.

In this context, the emergence of high-entropy nitrides (HENs) represents a paradigm shift in the development of next-generation SSACs.[17] HENs are single-phase compounds that contain multiple principal metal cations within the nitride lattice.[18] The high configurational entropy associated with incorporating many different elements stabilizes unique solid solutions and enables extensive tuning of the material's electronic structure.[19] This multi-cation strategy provides unprecedented control over optical and thermal properties while inherently improving resistance to oxidation, phase segregation, and thermal degradation. Their properties originate from the high-entropy, lattice distortion, sluggish diffusion, and cocktail effects, which collectively endow superior optical and thermal behavior. High configurational entropy reduces the driving force for phase separation, while lattice disorder raises migration barriers, suppressing coarsening and oxidation to ensure long-term stability. In addition, lattice distortion modifies bond lengths and electronic states, enabling defect-level absorption, and the synergistic cocktail effect often produces performance beyond the rule-of-mixture predictions. Leveraging entropy-driven stabilization and synergistic effects among diverse elements, HENs exhibit remarkable broadband solar absorption, ultra-high temperature stability, and robust mechanical performance.[4,20–24] These characteristics position them at the cutting edge of photothermal materials science. At the same time, the transition from well-studied binary nitrides to compositionally complex HENs brings new scientific and engineering challenges. Fundamental questions remain about how the increased chemical complexity, disorder, and lattice defects in HENs influence the photothermal performance and long-term behavior.[10] Furthermore, scalable and controllable synthesis methods for HEN coatings, as well as strategies to integrate them into practical substrates, are still under development and will be crucial for real-world deployment.[25]

This review provides a comprehensive overview of the evolution of SSACs, tracing developments from conventional
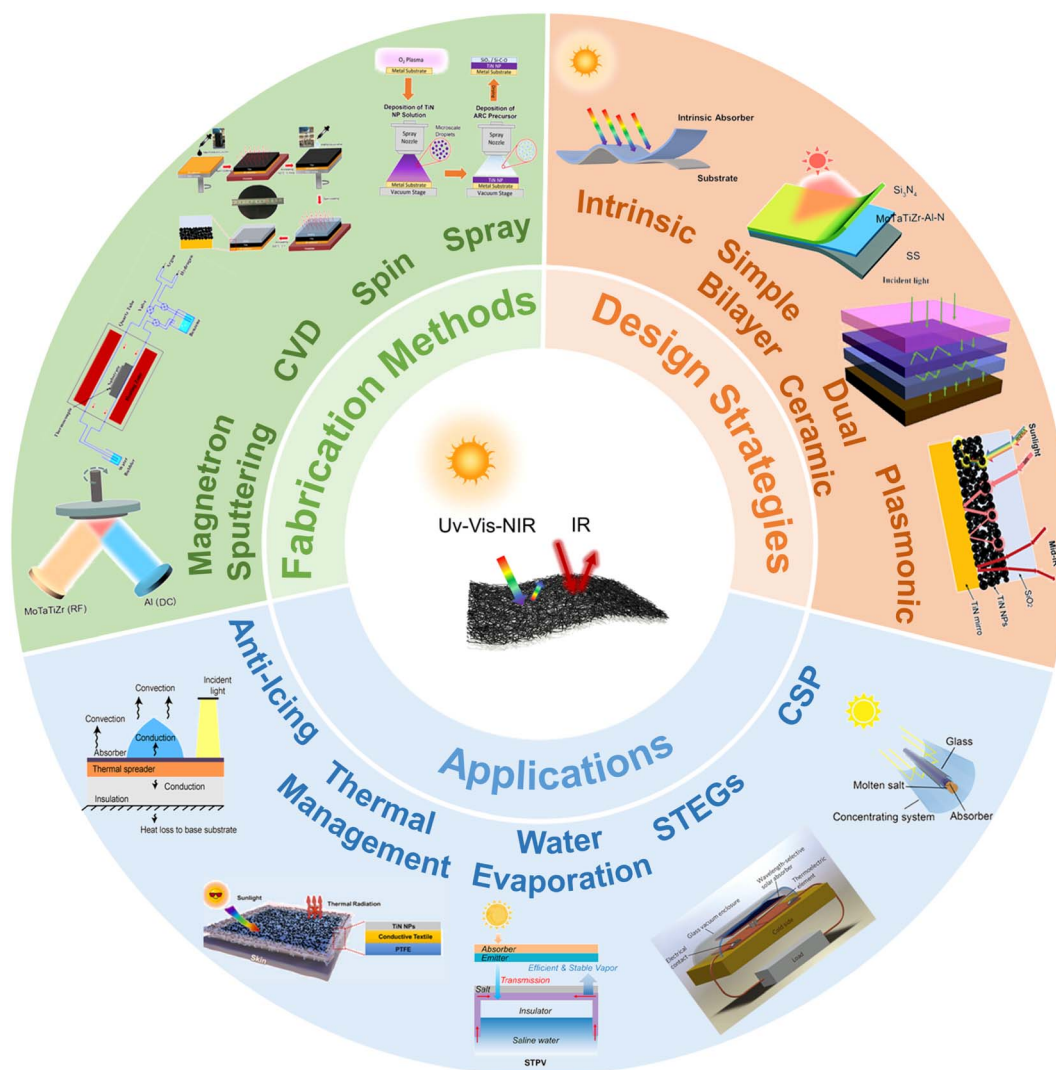

Fig. 1 Graphical overview of the review.

metal nitrides to state-of-the-art HENs (Fig. 1). We examine the underlying physical mechanisms and structure–property relationships that govern photothermal conversion in these materials, and we highlight recent breakthroughs in both classes of nitrides. Particular emphasis is placed on the advantages conferred by entropy engineering and multi-cation design, as well as the remaining bottlenecks and prospective research directions. By bridging the knowledge gap between classical nitrides and HENs, we aim to offer new insights and a forward-looking perspective on designing high-performance SSACs that can meet the challenges of next-generation solar–thermal technologies.

2 Mechanisms of photothermal conversion in nitrides

Efficient photothermal conversion relies on the intrinsic physical and chemical mechanisms by which materials absorb sunlight and convert photon energy into heat.[26] In solar absorber materials, two primary light–matter interaction mechanisms dominate: (i) plasma-related collective electron oscillations and (ii) discrete electronic transitions.[14,27] Additionally, structural disorder and entropy-driven effects play important roles in determining a material's photothermal behavior and robustness, especially in complex materials like HENs.[28]

2.1 Plasmonic and collective electron oscillations

In transition metal nitrides, incident photons can excite collective oscillations of free electrons, known as plasmon resonances, analogous to the well-known behavior in noble metals.[29,30] These excitations give rise to pronounced local electromagnetic fields at the nitride surface and can be broadly categorized into propagating surface plasmon polaritons traveling along metal–dielectric interfaces and localized surface plasmons confined to nanoscale features. When the incident light's wavelength coincides with the resonance frequency of these collective oscillations, strong light absorption is observed, typically as a distinct peak in the absorption spectrum (Fig. 2a). Transition metal nitrides such as TiN, ZrN, and HfN have attracted significant attention as plasmonic materials due to their visible-to-near-infrared resonance characteristics and high

thermal and chemical stability.[31,32] Unlike conventional noble metals, nitrides maintain their plasmonic response under extreme conditions, making them more suitable for durable solar–thermal applications. However, like their noble metal counterparts, traditional nitride-based plasmonic absorbers usually display relatively narrow absorption bands, which limit their efficiency for broadband solar harvesting. While nano-structuring strategies, such as creating arrays of nanoparticles or complex patterned films, can broaden and tailor absorption bands, these approaches often require sophisticated, high-cost fabrication processes.

High-entropy materials present an emerging and potentially scalable pathway to overcome the bandwidth limitations inherent in binary or ternary nitride plasmonics.[33,34] By incorporating multiple metallic elements into a single lattice, those materials can combine several distinct plasmon resonance frequencies, each arising from different constituent elements. The resulting superposition of multiple resonant modes leads to broadened and overlapping absorption features, yielding a more uniform and extended absorption profile across the solar spectrum.[35] In theory, this compositional complexity allows HENs to realize rich, broadband plasmonic responses without the need for elaborate nanofabrication, making them highly attractive for practical large-area coatings. It is important to note, however, that the plasmonic properties of high-entropy materials are still at an early research stage. While the concept of multi-resonant, broadband absorption is theoretically compelling, systematic experimental investigations and detailed understanding of plasmonic behavior in such materials remain limited.

2.2 Electronic transitions and band structure engineering

Beyond collective oscillations, photon absorption in a material also occurs via electronic transitions where electrons move between energy levels.[36] In photothermal materials, these electronic absorption processes are of two main types: intraband and interband transitions. Intraband transitions occur within the same energy band, typically within the conduction band of a semiconductor. Free charge carriers absorb photons and are excited to higher energies within the band, often with assistance from phonons (lattice vibrations) to conserve the momentum.[37] This intraband absorption mechanism is
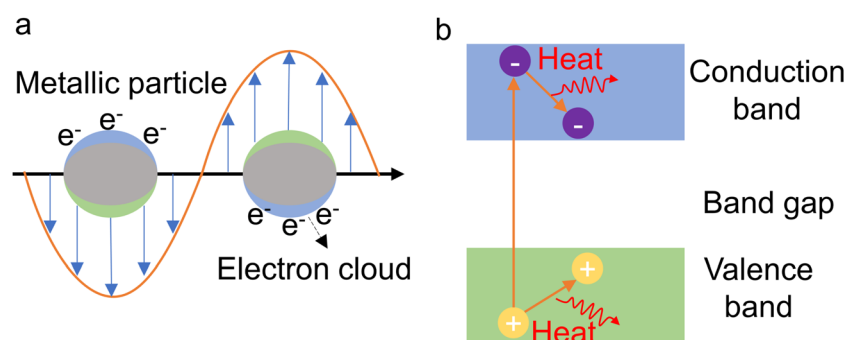

Fig. 2 Schematic illustration of (a) the localized surface plasmon resonance effect and (b) absorption via interband electronic transitions.

significant in materials with high free-electron concentrations, such as metals or highly doped semiconductors, and manifests as a broad absorption that increases toward longer wavelengths.[38] Interband transitions, on the other hand, involve electrons jumping from a lower energy band (like a valence band) to a higher energy band (conduction band) when they absorb a photon whose energy exceeds the bandgap (Fig. 2b). The efficiency and spectral range of interband absorption depend strongly on the bandgap energy and the detailed electronic band structure of the material, which can be tuned through composition and structure.

High-entropy materials with their multi-principal-element composition and intrinsic lattice disorder, present unique opportunities for band structure engineering to enhance photon absorption.[39,40] The random distribution of different cations in the lattice creates a complex potential landscape. This often leads to bandgap narrowing and can introduce localized states within the bandgap. Additionally, the presence of multiple elements and the associated lattice strain can increase the density of electronic states near the Fermi level. In practical terms, these effects allow HENs to absorb lower-energy photons that a wide-bandgap conventional nitride might not. Consequently, HENs often exhibit broader absorption spectra and enhanced photothermal conversion efficiency compared to their single-component counterparts.[41] By carefully selecting and combining elements, researchers can tailor the band structure of HENs to optimize their spectral absorption profile for solar–thermal applications.

2.3 Role of defects and disorder

Structural defects, such as vacancies and dislocations, have a significant influence on the photothermal properties of absorber materials. In high-entropy systems, the incorporation of multiple different cations inherently leads to a high degree of lattice distortion and a high concentration of point defects.[42] This pronounced disorder can be advantageous for photothermal conversion in several ways.

First, defects introduce additional electronic states within the bandgap of the material. These defect states can act as stepping stones for electrons, enabling the absorption of sub-bandgap photons.[43,44] This means a defective or disordered structure can capture lower-energy solar photons that an ideal crystal might transmit, thus broadening the absorption spectrum. These defect-related absorptions, although may not lead to useful electronic excitation for photovoltaics, are perfectly useful for photothermal conversion because they still generate heat. Second, defects and disorder facilitate non-radiative recombination of excited charge carriers. In a photothermal absorber, once a photon is absorbed and excites an electron, it is often preferable for that electron to quickly release its energy as heat rather than re-radiating it as light. Defect sites provide pathways for such non-radiative relaxation, efficiently converting the absorbed photon energy into thermal vibrations in the lattice. Third, the presence of high disorder can improve thermal stability. In HENs, the complex and irregular atomic arrangement effectively pins the microstructure by inhibiting long-range atomic diffusion and restricting the movement of dislocations.[45] As a result, processes that normally degrade a material at high temperatures, like grain growth, phase segregation, or diffusion of atoms to form new phases, are significantly slowed down. This is sometimes referred to as the sluggish diffusion effect in high-entropy materials. In practical terms, a HEN coating is less likely to undergo structural changes when exposed to prolonged high temperatures, which means its optical and mechanical properties remain stable during operation (Fig. 3a).

Overall, the high density of defects and lattice disorder in HENs not only broadens and strengthens optical absorption but also underpins the material's excellent stability under harsh conditions.[46] This combination is highly desirable for SSACs that need to operate reliably over long times in demanding solar–thermal environments.

2.4 Entropy-driven thermal stability

Thermal stability is a crucial requirement for solar absorber materials, as they must endure intense solar irradiation and high operating temperatures without significant degradation.[47] Traditional ceramic nitrides already possess strong covalent bonding and high melting points, which give them a degree of inherent thermal robustness. HENs amplify these traits through entropy-driven effects.
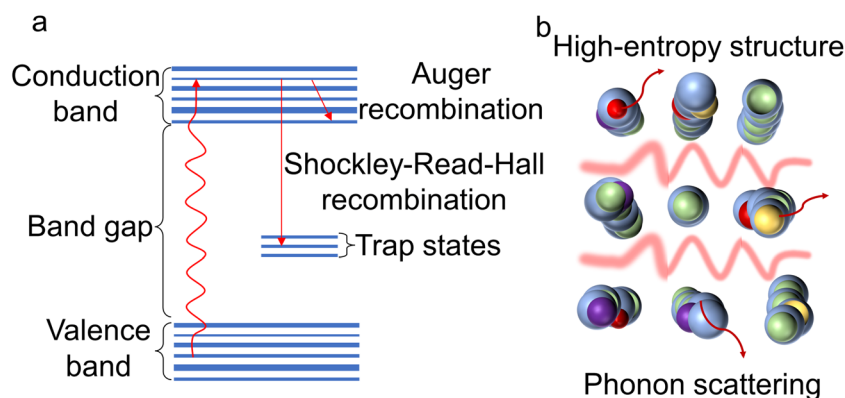

Fig. 3 Schematic illustration of (a) the influence of defects on the electronic band structure and (b) enhanced phonon scattering.

In an HEN, the random distribution of multiple different metal atoms in the lattice leads to a kind of "cocktail" of atomic sizes and bonding preferences. This chemical disorder has two notable consequences for thermal behavior. First, it impedes atomic mobility. Because the lattice lacks a simple, repeating pattern, it becomes difficult for atoms to diffusively hop from one place to another. This suppression of diffusion means that, even at elevated temperatures, HENs are resistant to processes like phase separation where different elements would normally segregate or grain coarsening where small crystalline grains merge into larger ones. Essentially, the material is kinetically trapped in its disordered state, which helps maintain its original microstructure and composition at high temperatures.

Second, the disorder in HENs increases phonon scattering. Phonons are the carriers of heat in a crystal.[48,49] In an ordered crystal, phonons can travel relatively freely, which contributes to higher thermal conductivity. In a disordered, multi-element lattice, however, phonons frequently scatter off of the mass fluctuations and strain fields caused by the different atoms. This scattering reduces the mean free path of phonons, effectively lowering the lattice thermal conductivity (Fig. 3b). For SSACs, lower thermal conductivity can be beneficial because it helps confine the heat near where it is generated rather than letting it rapidly conduct away into the substrate. Localized heat contributes to maintaining a high temperature at the absorber's surface and improves the efficiency of applications like steam generation or thermoelectric coupling. Together, these entropy-driven effects mean that HEN coatings can remain stable and maintain performance under conditions that would cause conventional coatings to fail. They can better resist thermal shock and remain phase-stable even after many heating–cooling cycles. The combination of suppressed degradation and reduced heat loss makes them particularly well suited for long-term operation in solar–thermal systems.

In summary, the superior photothermal performance of modern nitride-based SSACs arises from a confluence of mechanisms. Collective plasmonic oscillations enable strong, broadband solar absorption. Engineered electronic band structures and abundant defects extend absorption deeper into the infrared and ensure that absorbed photons are efficiently converted to heat. Meanwhile, the intrinsic disorder and high entropy in HENs confer exceptional thermal stability and longevity by preventing the usual high-temperature degradation pathways. A deep understanding of these fundamental processes is essential for the rational design of next-generation SSACs. By mastering how the composition and structure influence plasmonic response, electronic transitions, and thermal transport, researchers can tailor SSACs to achieve nearly ideal selectivity and durability.

3 Spectral selective mechanisms

3.1 Solar absorptivity

When light interacts with a material's surface, it can be reflected, transmitted, or absorbed (Fig. 4a).[50] According to the law of conservation of energy, the sum of energies corresponding to these three processes must equal the total incident light energy, which is typically normalized to unity. This relationship can be expressed as:

$$A_\lambda + R_\lambda + T_\lambda = 1 \tag{1}$$

where A_λ, R_λ, and T_λ are, respectively, the energies absorbed, reflected, and transmitted by the material at wavelength λ. For opaque materials, $T_\lambda = 0$. Therefore, the absorption can be determined from reflectance measurements. The spectral absorptance at a specific wavelength is defined as the ratio of absorbed to incident radiation. Since solar energy is predominantly distributed in the UV-vis-NIR range (0.3–2.5 μm), the total solar absorptivity is calculated as:

$$\alpha(\theta) = \frac{\int_{0.3}^{2.5} (1 - R_\lambda) G_\lambda(\lambda) d\lambda}{\int_{0.3}^{2.5} G_\lambda(\lambda) d\lambda} \tag{2}$$

where λ is the wavelength, θ is the angle of incidence, and $G_\lambda(\lambda)$ denotes the solar spectral irradiance under AM1.5 conditions. This integral quantifies the fraction of solar energy absorbed by a material, making solar absorptivity a key parameter in evaluating the efficiency of SSACs.
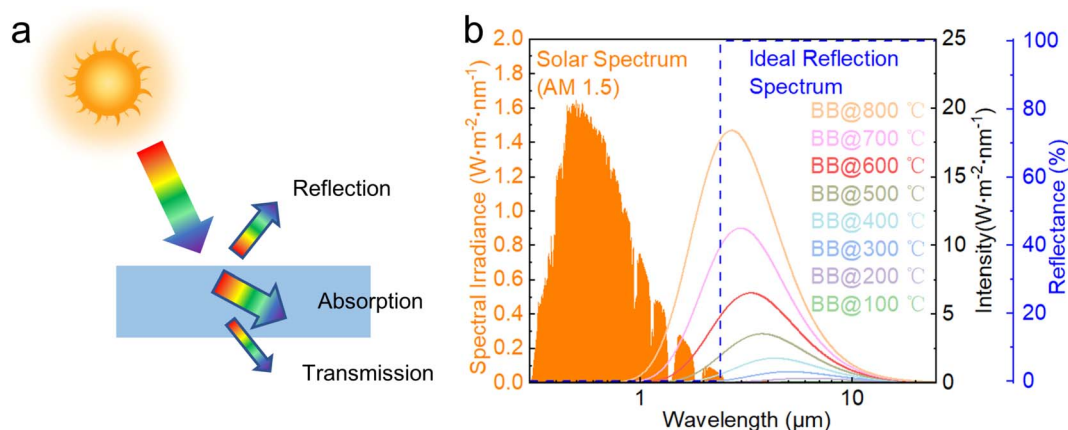

Fig. 4 (a) Schematic depiction of surface phenomena occurring in materials under light exposure. (b) Illustration of the ideal reflectance spectrum for SSACs at a working temperature of 400 °C.

3.2 Thermal emissivity

Thermal emissivity is a fundamental property describing a material's ability to emit electromagnetic radiation, rooted in blackbody theory. The spectral distribution of blackbody radiation is governed by Planck's law:

$$E_{b\lambda,\text{per}}(\lambda, T) = \frac{8\pi hc}{\lambda^5 \exp\left(\dfrac{hc}{\lambda k_B T} - 1\right)} \tag{3}$$

where $E_{b\lambda,\text{per}}(\lambda, T)$ is the spectral radiance at wavelength λ and temperature T, c is the speed of light, k_B is Boltzmann's constant, and h is Planck's constant. The Stefan–Boltzmann law states that the total emissive power of a blackbody scales with the fourth power of its temperature:

$$E_b(T) = \int_0^\infty E_{b\lambda,\text{per}}(\lambda, T)d\lambda = \sigma T^4 \tag{4}$$

The thermal emissivity (ε) of a material is defined as the ratio of radiation emitted by the material to that of an ideal blackbody at the same temperature. According to Kirchhoff's law, at thermal equilibrium, the hemispherical emissivity $\varepsilon_\lambda(\lambda)$ equals to the hemispherical absorptivity $\alpha_\lambda(\lambda)$ at each wavelength. Thus, the total emissivity at temperature T can be determined as:

$$\varepsilon(T) = \frac{\int_{0.76}^{25} [1 - R_\lambda(\lambda)]E_{b\lambda,\text{per}}(\lambda)d\lambda}{\int_{0.76}^{25} E_{b\lambda,\text{per}}(\lambda)d\lambda} \tag{5}$$

For an ideal SSAC, the reflectance spectrum should ideally exhibit a step-like profile: zero reflectance (maximum absorption) below the cut-off wavelength and unity reflectance (minimum absorption/emission) above it. At higher temperatures, the cut-off wavelength shifts to shorter values (Fig. 4b). The ratio of solar absorptivity to thermal emissivity (α/ε) is often used as a metric to evaluate spectral selectivity.

3.3 Photothermal conversion efficiency

In solar–thermal applications, the photothermal conversion efficiency is a critical parameter for assessing the performance of SSACs and guiding the absorber design.[14,51,52] The photothermal conversion efficiency can be expressed as:

$$\eta_{\text{thermal}} = B\alpha - \frac{\varepsilon\sigma\left(T^4 - T_0^4\right)}{CI} \tag{6}$$

where σ is the Stefan–Boltzmann constant, T is the working temperature, T_0 is the ambient temperature, C is the concentration factor, I is the incident solar flux, and B denotes the transmittance of the protective glass envelope (typically 0.91).[53]

4 Fabrication methods of nitride-based SSACs

Translating these material advantages into real-world devices requires fabrication techniques that can produce high-quality nitride coatings with precise control over composition, microstructure, and thickness. A variety of synthesis and deposition methods have been explored to create both conventional and HEN absorber layers.[10,22] Each fabrication approach offers distinct advantages in terms of film quality, scalability, and complexity. In this section, we review the principal fabrication methods for nitride-based SSACs and discuss representative examples of how each method has been used to achieve superior photothermal performance.[21,54–57]

4.1 Magnetron sputtering

Magnetron sputtering is one of the most widely used techniques for depositing nitride thin films, including HEN coatings.[58,59] It is a physical vapor deposition (PVD) process in which energetic ions, usually from a plasma of an inert gas like argon, bombard a solid target composed of the desired coating material.[60] Atoms are knocked off from the target and then condense onto a substrate, forming a thin film. The process typically occurs in a vacuum chamber and involves three main steps: (1) generating a plasma and sputtering target atoms, (2) transporting these atoms through the chamber, and (3) their condensation and growth into a film on the substrate. Magnetron sputtering allows for excellent control over film thickness, composition, and uniformity.

Employing reactive gases, such as introducing N_2/O_2 during the sputtering of a metal target, enables the direct synthesis of nitrides or oxynitrides with exact stoichiometry (Fig. 5a). Both direct current (DC) and radio-frequency (RF) power can be used; DC sputtering is common for conducting targets, while RF sputtering can be used for insulating or compound targets. The technique is scalable to large areas and can produce coatings with high purity and good adhesion, making it attractive for both laboratory and industrial-scale production of absorber coatings.[61] Numerous studies demonstrate the effectiveness of magnetron sputtering for fabricating advanced SSACs. For example, co-sputtering from double targets has been used to create HEN films with compositions such as ZrNbMoWN and MoTaTiCrAlN.[20,21] These sputtered HEN coatings have achieved solar absorptance above 0.92 with low thermal emittance of $\sim$0.05–0.20 in the infrared region, showcasing their potential for CSP and other high-temperature applications. In particular, the MoTaTiCrAlN-based SSAC deposited by magnetron sputtering maintained over 92% absorptance even after hundreds of hours at 650 °C, far outperforming a comparable binary nitride film.[21] Magnetron sputtering also permits tuning of the microstructure through deposition parameters. Adjusting factors like substrate temperature, gas pressure, or bias voltage can influence the grain size, density, and texture of the nitride film. For instance, reactive RF sputtering has been used to grow highly oriented aluminum nitride (AlN) coatings with a columnar nanostructure on silicon wafers, yielding smooth, dense films without cracks.[62]

4.2 Chemical vapor deposition

Chemical vapor deposition (CVD) is a versatile and widely used technique for producing high-purity, conformal films.[63] In a typical CVD process, one or more volatile precursors, such as
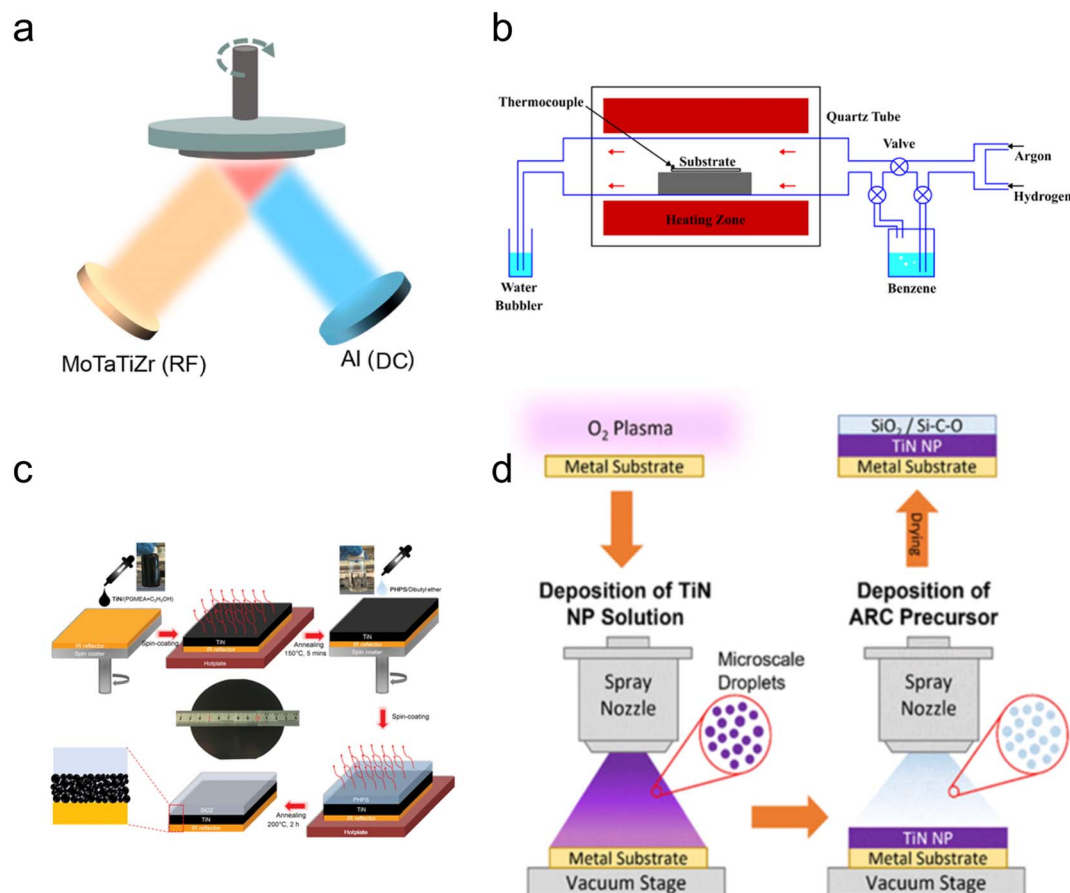
Fig. 5 Fabrication method for SSACs. Schematic illustrations of (a) magnetron sputtering,[21] Copyright 2022, Elsevier. (b) CVD,[54] Copyright 2014, Wiley-VCH; (c) spin coating,[56] Copyright 2020, Wiley-VCH and (d) spray coating.[57] Copyright 2025, Engineered Science.

metal halides or organometallic compounds for the metal source, and ammonia or nitrogen-containing gases for the nitrogen source, are introduced into a reaction chamber.[64] Upon reaching the heated substrate, these precursors undergo controlled chemical reactions or decomposition, resulting in the formation of a dense, uniform solid film.[65] CVD is generally performed at reduced pressures and elevated temperatures, which promote film crystallinity and compositional control (Fig. 5b). CVD offers several key advantages for the fabrication of SSACs, including accurate thickness control, the ability to coat substrates with complex geometries, and excellent adhesion to underlying materials.

Historically, CVD has enabled the development of advanced SSACs for solar energy conversion. Early foundational work by Erben and colleagues in the 1980s established CVD as a viable process for functional SSACs.[66] More recently, Selvakumar et al.[54] demonstrated a tandem absorber comprising Ti/AlTiO/CoO/CNTs layers on 304 stainless steel (SS) via CVD, which exhibited a solar absorptance (α) of 0.95, an emittance (ε) of 0.20, and robust thermal stability up to 650 °C in vacuum. Additionally, the integration of CVD with other deposition techniques allows for the creation of sophisticated multilayer architecture. Rebouta et al.[55] fabricated a TiAlN/TiAlON/SiO$_2$ SSAC by sequentially depositing TiAlN and TiAlON layers via

magnetron sputtering in Ar/N$_2$/O$_2$ atmospheres, followed by the growth of a SiO$_2$ antireflection (AR) layer using CVD with an OMCTS precursor. The individual layer thicknesses (65 nm TiAlN, 51 nm TiAlON, and 100 nm SiO$_2$) were optimized through optical simulations to achieve high solar absorptance (95.5%) and low thermal emittance (5%). This multilayer coating displayed excellent thermal stability after prolonged annealing, underscoring its suitability for demanding solar–thermal applications.

4.3 Solution-based coating

Solution-based deposition techniques, such as spin coating and spray coating, provide relatively simple and cost-effective routes to create SSACs from liquid precursors or nanoparticle suspensions. These methods are particularly attractive for lab-scale prototyping and can be scaled for large-area or roll-to-roll processing in some cases.

In a spin-coating process, a small amount of liquid solution is dropped onto the substrate, which is then rapidly rotated. Centrifugal force spreads the liquid into a thin, even layer (Fig. 5c). The thickness of the resulting wet film depends on the spin speed, spin time, and viscosity and concentration of the solution. After coating, the film typically undergoes drying and curing or annealing steps to solidify it and, if needed, convert it

into the desired material. Spin coating excels at producing uniform thin films on flat substrates (wafers and glass slides) with fine control over thickness from a few nanometers to a few microns. It is widely used for sol–gel processes, where a solution containing molecular or nanoparticle precursors is deposited and then transformed into a ceramic coating.

Spin coating has been used in the development of SSACs where the absorber can be formed from a precursor layer. For instance, a metal salt solution can be spin-coated and then thermally treated in ammonia or nitrogen to form a nitride layer. Alternatively, pre-formed nanoparticles can be dispersed in a solvent and spin-coated to create a porous absorbing layer that is later infiltrated or capped with another material. In one notable example, TiN nanoparticles with ∼20 nm in size were dispersed in a solvent and spin-coated onto a substrate to form a thin absorbing film. Subsequently, an AR layer was spin-coated on the top surface.[56] This layer was derived from a liquid polysilazane precursor which would transform into SiO_2 when heated. The result was a nanoparticle-based SSAC that achieved high spectral selectivity and maintained stability up to around 727 °C. While spin coating in itself is mostly a laboratory technique, it proves extremely useful for rapidly exploring new material combinations and layer structures in photothermal research.

Spray coating is a technique where a liquid precursor is atomized into fine droplets and sprayed onto a surface, typically using a nozzle and a carrier gas (Fig. 5d). It is well suited for coating larger areas and non-flat objects, and it can be performed under ambient conditions for many materials. One variant, ultrasonic spray coating, uses high-frequency vibrations to generate a very uniform mist of droplets, which leads to more uniform films.

Researchers have demonstrated ultrasonic spray coating to create SSACs. In a representative study, a suspension of TiN nanoparticles in a volatile solvent was sprayed onto metal substrates to form the absorber layer. By optimizing parameters like the solution concentration, spray flow rate, nozzle-to-substrate distance, and raster pattern of the spray, they achieved a uniform ∼100 nm thick TiN coating over areas as large as 20×20 cm². After depositing the absorber, a diluted polysilazane solution was similarly sprayed on and converted to a thin SiO_2-based AR topcoat. The resulting coatings exhibited high solar absorptance up to ∼90% and extremely low emittance of ∼2% in the infrared region, rivaling the performance of more expensive commercial SSACs. Importantly, this was accomplished using a low-cost, ambient process, highlighting the potential of solution-based methods for scalable manufacturing.[57] The spray-coated layers were also mechanically robust and adhered well, even under thermal cycling, indicating that carefully formulated inks can yield durable photothermal coatings.

In summary, solution-based coating techniques provide a complementary approach to vacuum-based methods like PVD and CVD. They are generally simpler and can be scaled over large or flexible substrates, although achieving very high precision and ultra-pure films can be more challenging. In the development of nitride absorber coatings, these methods have enabled fast prototyping and the incorporation of nanomaterials like plasmonic nitride nanoparticles into coatings. Continued improvements in ink formulations and post-deposition treatment, e.g., better sintering processes, may further enhance the performance and applicability of solution-deposited SSACs.

5 Design strategies for SSACs

SSACs must be engineered to capture as much solar radiation as possible while minimizing emissions of thermal radiation.[10] Traditional metal nitrides like TiN, ZrN, CrN, etc. offer strong intrinsic absorption and good thermal stability,[67,68] but by themselves they rarely achieve the ideal balance of high solar absorptance and low infrared emittance. To meet the stringent requirements of advanced solar–thermal systems, researchers have developed a variety of design strategies that combine material selection with clever architectural engineering.[12] In this section, we discuss the main design approaches for nitride-based SSACs, from simple single-layer films to complex multi-layer and nanostructured systems, highlighting how both conventional nitrides and emerging HENs are employed to optimize the optical properties, thermal stability, and spectral selectivity (Table 1).[69–71]

5.1 Intrinsic SSACs

The principle behind intrinsic SSACs is tied to the material's band structure (Fig. 6a).[91] Many semiconductors and semi-metallic compounds exhibit strong absorption of photons with energies higher than a specific threshold set by their bandgap or plasma frequency, while they remain reflective or transparent to light with longer wavelengths.[92–95] In short, when incident light has a wavelength shorter than the material's cutoff, meaning the photon energy exceeds the bandgap, electrons in the material are excited from the valence band to the conduction band, which converts the photon energy into heat. This leads to strong absorption of shorter-wavelength light. However, for longer wavelengths where the photon energy is below the bandgap, intrinsic absorption decreases, and the material typically reflects or transmits the light rather than absorbing it. This behavior creates a form of spectral selectivity inherently: high absorption in the solar spectrum and low emission in the IR region.

Some transition metal nitrides can serve as intrinsic SSACs by virtue of their electronic structure. For example, CrAlN films can act as efficient solar absorbers on their own. In one study,[96] DC-sputtered CrAlN films showed high solar absorptance across 300–2600 nm (Fig. 6b). The films formed a stable NaCl-type crystal structure with well-oriented grains, and their semi-conducting nature (high electrical resistivity) contributed to inherent low thermal emittance (Fig. 6c). This combination of strong intrinsic absorption and excellent oxidation resistance makes CrAlN a promising single-layer absorber for high-temperature applications. Similarly, TiAlN coatings have been explored as intrinsic absorbers.[69] TiAlN thin films exhibit a broad, strong absorption band around the visible region

Table 1 Comparison of the structures, fabrication methods, and performance of various SSACs

| Classes	Composition and structure	Fabrication method	α	ε	Thermal stability	Ref.
Intrinsic SSACs	TiAlN/Al	Magnetron sputtering	0.93	0.09 (100 °C)	—	69
	NbTiAlSiN$_x$	Magnetron sputtering	0.822	—	700 °C for 24 h under vacuum	72
Simple bilayer structures	CrO$_x$N$_y$/SnO$_2$	Reactive sputtering	0.932	0.069 (278 °C)	278 °C for 600 h under air	73
	TiN/Al$_2$O$_3$	Magnetron sputtering	0.92	0.11 (82 °C)	500 °C for 5 h under vacuum; 200 °C for 2 h under air	74
	AlCrTaTiZrN/SiO$_2$(Si$_3$N$_4$)	Magnetron sputtering	0.916 (0.928)	0.051 (82 °C)	650 °C for 300 h under vacuum	75
	MoTaTiCr-Al-N/Si$_3$N$_4$	Magnetron sputtering	0.923	0.07 (82 °C)	750 °C for 168 h under vacuum	21
	AlTaTiZrN/Si$_3$N$_4$	Magnetron sputtering	0.927	0.08 (82 °C)	750 °C for 120 h under vacuum	24
	AlCrMoTaTiN/Al$_2$O$_3$	Magnetron sputtering	0.929	0.082 (82 °C)	600 °C for 100 h under vacuum; 300 °C for 2 h under air	59
Dual ceramic and graded composite structures	TiAlN/TiAlON/Si$_3$N$_4$	Magnetron sputtering	0.92	0.08 (82 °C)	600 °C for 2 h under air	76
	NbAlN/NbAlON/Si$_3$N$_4$	Magnetron sputtering	0.956	0.07 (82 °C)	450 °C for 116 h under air	77
	W/WSiAlN$_x$/WSiAlO$_y$N$_x$/SiAlO$_x$	Magnetron sputtering	0.96	0.105 (400 °C)	600 °C for 300 h under vacuum; 450 °C for 400 h under air	78
	TiAlSiN/TiAlSiO/SiO$_2$	Magnetron sputtering	0.96	0.05 (100 °C)	278 °C for 600 h under air	79
	Al/MoNbHfZrTiN/MoNbHfZrTiON/SiO$_2$	Magnetron sputtering	0.935	0.09 (82 °C)	450 °C for 2 h under vacuum	70
	AlCrTaTiZrN/Si$_3$N$_4$	Magnetron sputtering	0.965	0.086 (82 °C)	600 °C for 10 h under vacuum	71
	W/TiAlN/TiAlSiN/TiAlSiON/TiAlSiO$_2$	Magnetron sputtering	0.954	0.07 (82 °C)	350 °C for 1000 h under air	80
	TiN/TiNO/ZrO$_2$/SiO$_2$	Magnetron sputtering	0.922	0.17 (727 °C)	727 °C for 150 h under Ar	81
	WAlN/WAlON/Al$_2$O$_3$	Magnetron sputtering	0.958	0.08 (82 °C)	500 °C for 2 h under air	82
	HfMoN/HfON/Al$_2$O$_3$	Magnetron sputtering	0.95	0.14 (82 °C)	—	83
	HfMoN(H)/HfMoN(L)/HfON/Al$_2$O$_3$	Magnetron sputtering	0.95	0.14 (82 °C)	500 °C for 7 h under air	84
	Al/NbTiSiN/NbTiSiON/SiO$_2$	Magnetron sputtering	0.931	0.12 (400 °C)	550 °C for 100 h under vacuum; 500 °C for 2 h under air	85
Plasmonic and metamaterial SSACs	AlCrTaTiZrN(H)/AlCrTaTiZrN(L)/Si$_3$N$_4$	Magnetron sputtering	0.962	0.088 (—)	—	86
	MoTaTiCrN(H)/MoTaTiCrN(L)/Si$_3$N$_4$	Magnetron sputtering	0.952	0.068 (82 °C)	600 °C for 300 h under vacuum	87
	TiN/TiAlON/TiO$_2$-SiO$_2$	Magnetron sputtering	0.95	—	600 °C for 7 h under air	88
	TiN/TiN nanoparticles/SiO$_2$	Spin coating	0.95	0.03 (100 °C)	727 °C for 150 h under vacuum; 627 °C for 150 h under air	56
	(NiCuCrFeSi)N	Magnetron sputtering	0.99	0.14 (400 °C)	—	89
	TiN/SiO$_2$	Spray coating	0.90	0.06 (25 °C)	—	90
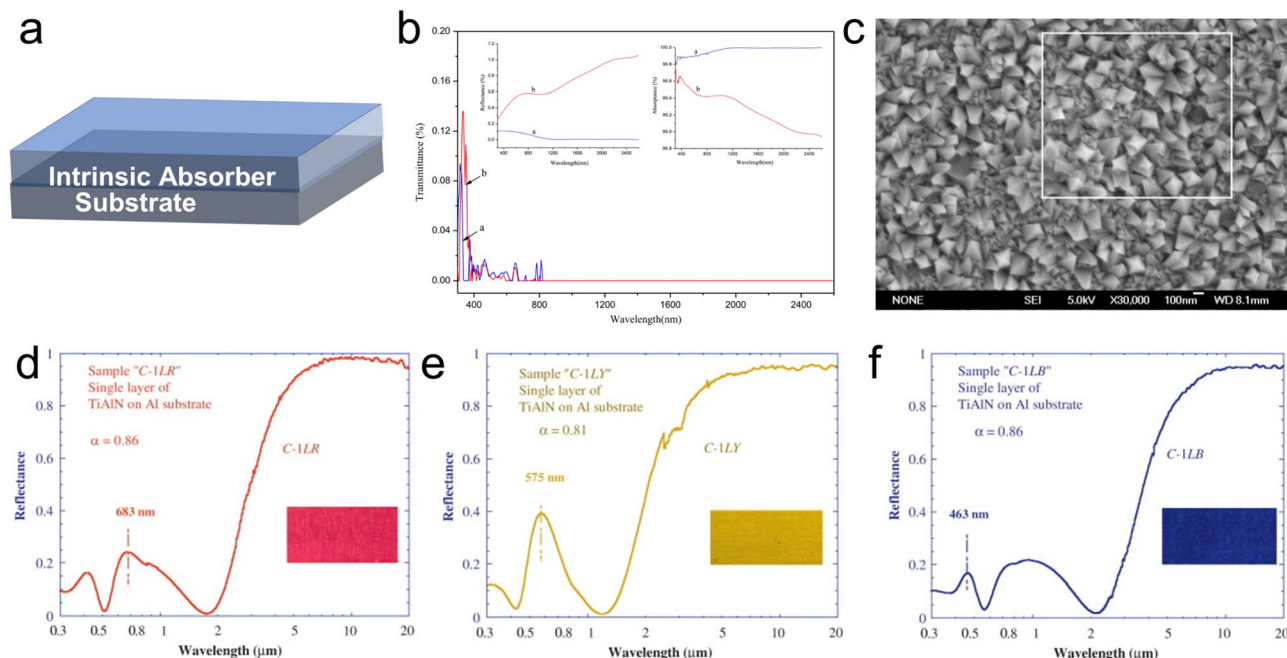
Fig. 6 Fundamentals and recent advances in intrinsic SSACs. (a) Structural schematic of intrinsic SSACs. (b) Transmittance, reflectance, and absorptance spectra and (c) SEM image of CrAlN films.[96] Copyright 2014, Elsevier. (d–f) Reflectance spectra of TiAlN SSACs with various colors.[69] Copyright 2010, Elsevier.

(~500 nm) due to their electronic band structure. Notably, TiAlN's optical properties can be tuned by composition and thickness, enabling not just high absorptance but also control over visible color. This demonstrated that by adjusting the TiAlN layer thickness, one can produce coatings of various colors while still maintaining decent spectral selectivity (Fig. 6d–f). This illustrates that intrinsic nitride absorbers can be versatile, even allowing aesthetic integration, although pure single-layer designs often involve trade-offs between appearance and absolute performance. A notable advancement was reported by Zhang et al.,[72] who prepared amorphous HENs NbTiAlSiN$_x$ via reactive DC magnetron sputtering. By varying the nitrogen flow rate during deposition, they achieved films with stable amorphous structures which demonstrated remarkable thermal stability up to 700 °C. The optimized films exhibited a maximum hardness of 20.5 GPa and high modulus values, along with smooth and dense morphologies. Optical characterization revealed strong solar absorption in the 0.3–2.5 μm range, making these films promising candidates for high-temperature CSP systems.

In practice, many metal nitrides demonstrate this effect to some extent. Unfortunately, most single materials do not have an ideal cutoff exactly tailored to the solar spectrum and also often suffer from either insufficient absorption or too much thermal emission. While intrinsic nitride coatings like CrAlN or TiAlN can achieve good optical performance, few materials alone can reach extreme spectral selectivity and thermal stability needed for top-tier solar thermal systems.[97] Even cutting-edge nitride ceramics and HENs, with all their compositional tuning, face this fundamental trade-off when used alone. To bridge the gap, a range of composites and multilayer design strategies have been developed. The most widely adopted approaches include adding an AR layer on top of an absorber to form a bilayer, using graded-index coatings or tandem cermet layers to gradually transition optical properties and trap light, and incorporating nanoscale structuring or metamaterials that exploit plasmonic resonances and interference effects for broadband absorption. Notably, HENs are compatible with all of these design strategies. One can use an HEN as the absorber layer in a bilayer design, or as a constituent of a cermet, or even fabricate a nanostructured film, offering new degrees of freedom to optimize performance. Below, we discuss each design strategy in detail, highlighting specific examples where both traditional nitrides and HEN materials have been used to realize superior spectral selectivity, thermal stability, and durability.

5.2 Simple bilayer structures

One of the simplest and most effective designs for SSACs is the bilayer structure. This consists of two layers: a bottom absorber layer that strongly absorbs solar radiation and a top dielectric AR layer that reduces reflective losses (Fig. 7a). Despite its simplicity, a well-designed absorber/AR bilayer can boost spectral selectivity compared to a bare absorber and simultaneously enhance thermal stability by preventing oxidation of the metal nitride underneath. The operating principle is that the AR, usually a transparent oxide with a low refractive index such as SiO$_2$, Al$_2$O$_3$, or Si$_3$N$_4$, is carefully tuned in thickness.[98] The typical thickness is about one quarter of a target wavelength in the middle of the solar spectrum, which creates destructive interference for reflected light and thus enables more sunlight
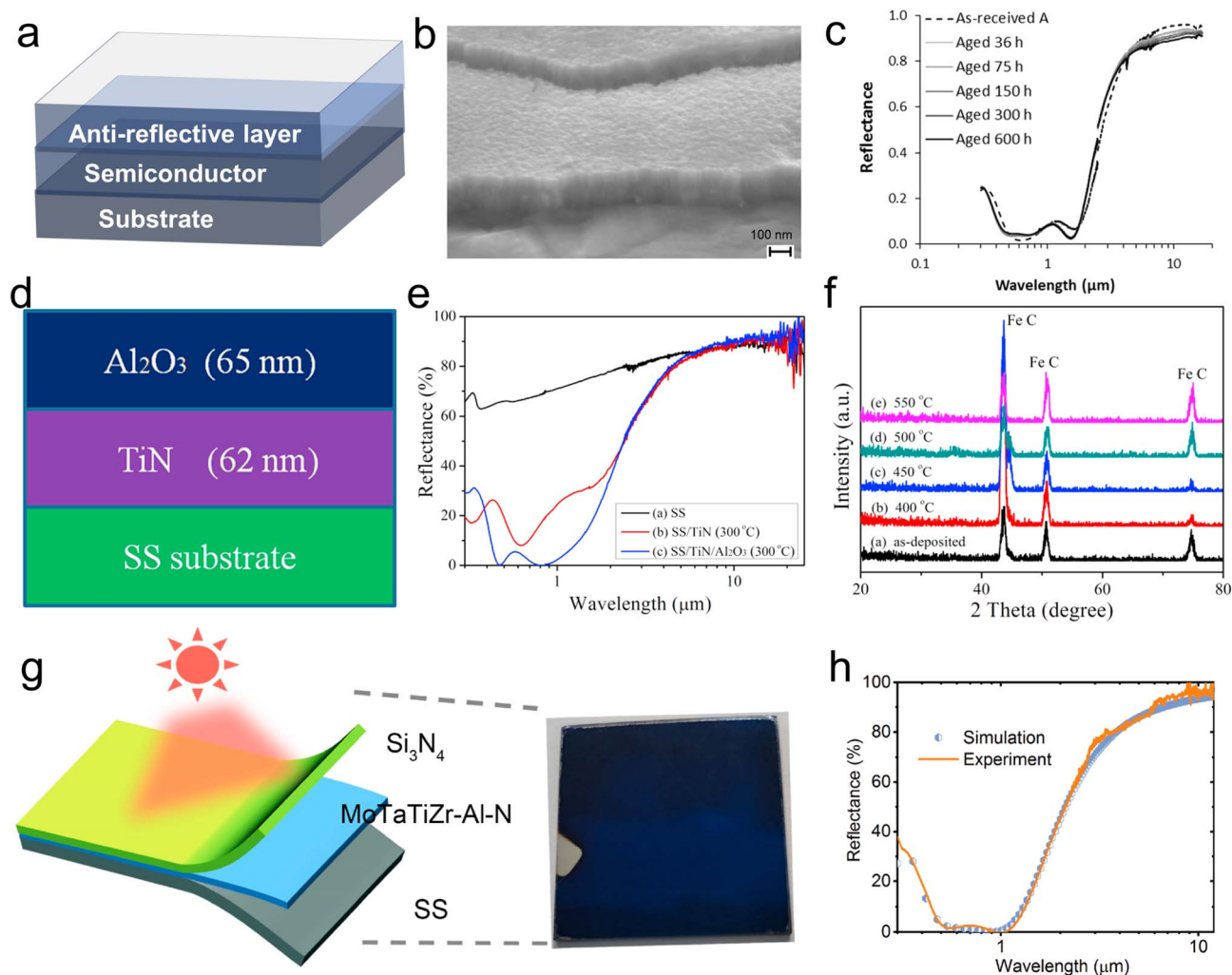
Fig. 7 Fundamentals and advances in simple double-layer SSACs. (a) Structural schematic of a typical bilayer structure. (b) Cross-sectional SEM image of CrO$_x$N$_y$/SnO$_x$ coatings. (c) Reflectance curves for CrO$_x$N$_y$/SnO$_x$ SSACs.[73] Copyright 2015, Elsevier. (d) Schematic of the SS/TiN/Al$_2$O$_3$ SSAC. (e) The reflectance spectra of SS/TiN/Al$_2$O$_3$ deposited at 300 °C. (f) XRD patterns of SS/TiN/Al$_2$O$_3$ SSACs before and after annealing at various temperatures in a vacuum.[74] Copyright 2017, Elsevier. (g) Schematic of the MoTaTiCr-Al-N-based SSAC. (h) Experimental and simulated reflectance spectra of the MoTaTiCr-Al-N-based SSAC.[21] Copyright 2022, Elsevier.

to pass through the coating and reach the absorber layer. At the same time, this dielectric layer, being transparent in the solar range but emissive neutral in the infrared region, doesn't add significant thermal emission.

Kotilainen et al.[73] reported such a bilayer design on copper substrates using reactive sputtering to deposit both the nitride absorber and the oxide AR. The CrO$_x$N$_y$ base layer provides strong absorption due to its metallic nitride nature and oxygen-tunable band structure, while the SnO$_2$ top layer transparent in the solar spectrum significantly cuts down reflectance. The optimized bilayer achieved a high solar absorptance of around ~0.90 and a low thermal emittance (~0.07 at 82 °C), which already meet the performance requirements for many solar thermal systems (Fig. 7b and c). An additional benefit of this design was improved thermal stability at moderate temperatures: the dense, columnar CrO$_x$N$_y$ layer acted as a diffusion barrier on the copper substrate, reducing degradation during

heating. However, at very high temperatures above ~400 °C, the copper from the substrate eventually interdiffused through the thin layers, leading to optical degradation and adhesion loss. Other researchers have implemented similar bilayer schemes with different material pairs. Gao et al.,[74] for instance, developed a tandem coating of TiN as the absorbing layer and Al$_2$O$_3$ as the AR layer on stainless steel (Fig. 7d). TiN, as discussed, is an excellent solar absorber due to its metallic luster that belies a high extinction coefficient in the visible/near-IR, and alumina is a common AR layer due to its transparency. The TiN/Al$_2$O$_3$ bilayer achieved solar absorptance around 0.92 and a thermal emittance of 0.11 (at 82 °C) (Fig. 7e). Importantly, it showed good thermal stability in a vacuum up to 500 °C for several hours with minimal performance drop, thanks to the robust nature of TiN and the protective Al$_2$O$_3$ capping (Fig. 7f).

Building on the success of conventional bilayers, researchers have started incorporating HENs into this design to push

performance limits further.[99,100] HEN thin films, containing multiple metal elements, often exhibit extremely stable single-phase structures and sluggish diffusion kinetics, which can suppress degradation mechanisms at high temperatures. He *et al.*[75] recently demonstrated a bilayer SSAC using an AlCrTa-TiZrN HEN absorber with a SiO_2 or Si_3N_4 top layer. The HEN was deposited by reactive sputtering from an alloy target, forming a single solid solution nitride that takes advantage of multi-element doping. This HEN absorber layer combined with a dielectric AR layer delivered an impressive solar absorptance of about 92–93% and an exceptionally low infrared emittance. More strikingly, the coating retained nearly identical optical properties even after being exposed to 650 °C for 300 h, a temperature and duration under which most traditional absorbers would have experienced significant oxidation or degradation. In another example, He *et al.*[21] prepared a co-sputtered HEN composed of Mo, Ta, Ti, and Cr with Al doping and then deposited a sputtered Si_3N_4 layer on top to form a bilayer structure (Fig. 7g). By adjusting the power supplied to each metal target during deposition, they achieved precise control over the composition of the HEN film, with a particular focus on regulating the Al content. The optimized HEN/Si_3N_4 bilayer achieved a solar absorptance of approximately 0.923 and a low emittance of around 0.07 at room temperature while demonstrating exceptional thermal stability (Fig. 7h). Such results highlight that HENs can serve as next-generation absorber layers in simple bilayer configurations, conferring superior resistance to oxidation and interdiffusion at high temperatures.

With only one absorber layer and one AR layer, these coatings maintain a simple design that is beneficial for large-scale manufacturing while still achieving both high efficiency and robust thermal stability. The bilayer approach provides a compelling balance between performance and complexity. It significantly improves upon single-layer SSACs by using interference to boost absorption and by shielding the absorber layer, yet it avoids the added intricacy of thicker multilayer stacks. Numerous studies on bilayer nitride coatings, from binary nitrides like TiN to multi-component and HENs, confirm that this straightforward architecture can achieve the necessary selective absorption and withstand the demanding environments of solar–thermal systems.

5.3 Dual ceramic and graded composite structures

While bilayers introduce one additional interface and layer, further enhancements in spectral selectivity can be achieved by more complex multilayer designs.[101] A prominent strategy uses tandem absorber layers with graded optical properties, often referred to as dual-ceramic structures. In this design, instead of a single homogeneous absorber layer, there are two (or more) absorber sub-layers, each typically a composite of metallic and dielectric components.[102] By varying the metal volume fraction or composition between the bottom and top absorber layers, one can create an effective gradient in the refractive index and absorption coefficient through the thickness of the coating. The bottom layer is usually more metallic using a higher metal

nanoparticle content or a conductive nitride, providing strong absorption and an infrared-reflecting base, whereas the upper absorber layer is more dielectric, which serves to impedance-match the lower layer to air and absorb the leftover light without adding too much reflectance. Often, beneath the absorbing layers, a fully reflective metal substrate or metallic back-layer like W or Mo is used to reflect any unabsorbed solar light back into the stack and to block thermal radiation from the substrate. The very top surface may still have a thin AR layer to minimize surface reflection and oxidation (Fig. 8a).

Early examples of dual-layer nitride absorbers used simple binary nitrides. For instance, a tandem of CrN and Al_2O_3 layers was tested (Fig. 8b).[68] Such coatings did achieve good initial optical selectivity, but their thermal stability was limited. The example tandem CrN/Al_2O_3 was only stable to about 400 °C in air before significant oxidation and performance loss occurred.[68] The relatively low stability was due to oxidation of CrN and perhaps diffusion or crystallization in the layers. To push stability higher, researchers found that doping and alloying the ceramic absorber layers are highly effective. By introducing additional elements into the nitride phases, one can improve both the optical properties and stability. For example, adding tungsten into AlN to form WAlN cermets (Fig. 8c),[103] or using multi-metal nitride particles like CrMoN,[104] NbMoN,[105] HfMoN,[83] or AlCrN[106] has yielded absorbers that survive to markedly higher temperatures.[84,103,105,107,108] Some dual-layer absorbers using complex nitrides have demonstrated stability up to ~600 °C. In one case, a tandem absorber with HfMoN-based cermet layers maintained excellent performance even after extended heating at 600 °C, far surpassing its binary-nitride counterparts.[84]

The inclusion of refractory metals (Hf, Mo, W, *etc.*) in the nitride appears to slow oxidation and can form protective oxide scales *in situ*.[109] This concept of multi-element doping is essentially a precursor to high-entropy design, where the nitride phase contains several different metals to maximize both the phase stability and the chance of forming a self-passivating oxide layer. A concrete illustration is the work of Wu *et al.*, who developed a tandem absorber by substituting NbTiN/NbTiON layers with Si-doped versions.[85] In their design, the bottom layer was a Si-doped nitride serving as the main absorber and the top layer was a Si-doped oxynitride. The introduction of a few atomic percent of silicon into the nitride matrix dramatically improved the oxidation resistance. After 2 h at 500 °C in air, the Si-doped tandem still had a solar absorptance around 0.92 and an emittance of ~0.13, whereas a similar coating without Si would have severely degraded. The mechanism is that silicon doping leads to the formation of a thin SiO_2-rich scale and stabilizes the fine nanostructure of the cermet, preventing grain growth and oxidation of the metallic components.

In another study, Zou *et al.*[110] utilized an AlCrSiN/AlCrSiON/AlCrO multilayer to achieve both high selectivity and stability (Fig. 8d). The presence of multiple elements in the absorber layers was credited with pinning grain boundaries and inhibiting grain growth up to 600 °C. Essentially, the mixed nitride/oxynitride structure remained a nano-composite and did not
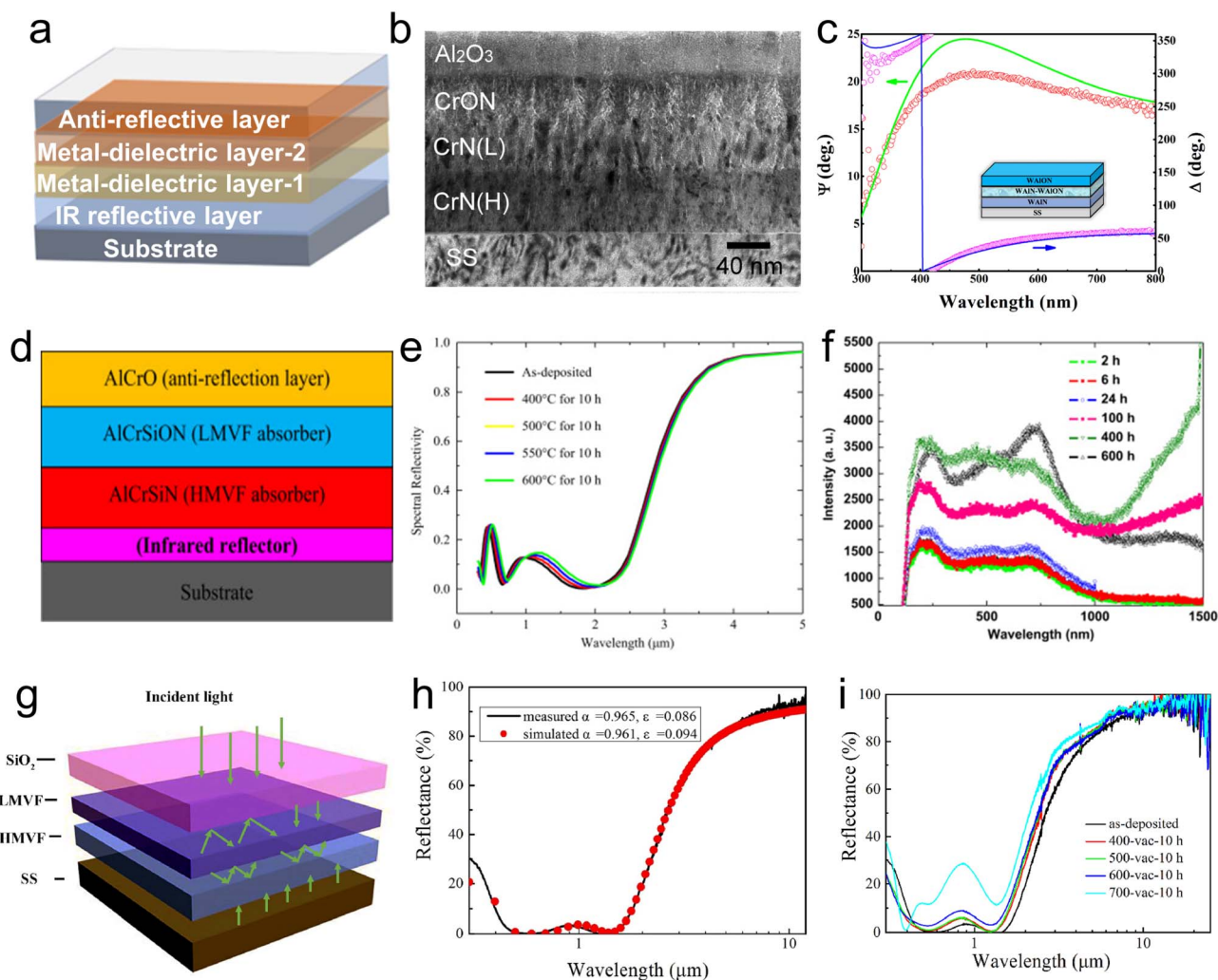
Fig. 8 Fundamentals and advances in gradient nitride ceramics–based SSACs. (a) Structural schematic of dual-ceramic and graded composite architecture. (b) TEM image of CrN(H)/CrN(L)/CrON/Al$_2$O$_3$.[68] Copyright 2016, Elsevier. (c) Ellipsometric data for the WAlN/WAlN–WAlON/WAlON SSAC.[103] Copyright 2017, Elsevier. (d) Schematic diagram of the AlCrSiN/AlCrSiON/AlCrO multilayers. (e) Reflectance spectra and (f) Raman spectra of the AlCrSiN/AlCrSiON/AlCrO SSAC before and after annealing treatments.[110] Copyright 2016, Elsevier. (g) Structural schematic of AlCrTaTiZrN-based SSACs. (h) Simulated and experimental spectra and (i) reflectance spectra of AlCrTaTiZrN-based SSACs before and after annealing.[71] Copyright 2020, Elsevier.

coarsen significantly after heating, which helped preserve its optical performance (Fig. 8e and f). Similarly, AlRjoub et al.[78] reported a four-layer tandem for CSP receiver tubes consisting of a W back-mirror, a high-absorbing WSiAlN$_x$ layer, a second absorbing layer of WSiAlON, and an AlSiO topcoat for AR and oxidation resistance. On stainless steel substrates, this stack delivered ~96% solar absorptance with ~10% emittance (at 400 °C) and withstood hours of heating at 450 °C in air (and up to 600 °C in a vacuum) with minimal degradation. In another advanced design, the team also demonstrated a TiAlSiN/TiAl-SiON/SiO$_2$ triple-layer stack that reached about 96% absorptance and only 5% emittance.[79] By carefully tuning the sputtering conditions, they produced a nitride layer and a slightly oxygenated nitride layer with complementary optical properties. These cases demonstrate a general principle: multi-component nitride absorbers show superior thermal stability

because they can form complex, adherent oxides and maintain structural integrity at temperatures where simpler SSACs fail.

To further push the stability of dual-ceramic absorbers, researchers have turned to high-entropy concepts. By introducing multiple metals into the nitride cermet layers, the structure can maintain its selective performance at higher temperatures. For instance, Gao et al.[70] developed a multilayer high-temperature colored SSAC coating based on the HEA MoNbHfZrTi. Using reactive RF magnetron sputtering, they fabricated a four-layer structure consisting of Al, MoNbHfZrTiN, MoNbHfZrTiON, and SiO$_2$. By fine-tuning the deposition parameters and gas flow rates, they achieved a compositional gradient and tailored the absorption edge toward longer wavelengths. The optimized Al/MoNbHfZrTiN/MoNbHfZrTiON/SiO$_2$ coating exhibited a high solar absorptance of 0.935 and a low emittance of 0.09. Notably, by adjusting the thicknesses of the

MoNbHfZrTiON and SiO$_2$ layers, a variety of colored SSACs with excellent spectral selectivity were obtained, as confirmed by chromaticity measurements. The coating retained high optical performance and visible color tunability, highlighting the promise of HENs for multifunctional, high-performance SSACs with customizable optical properties. He et al.[71] designed and fabricated a novel SSAC based on AlCrTaTiZrN using a multi-layer architecture. The coating features sequential layers of high and low metal volume fraction (HMVF and LMVF) AlCrTaTiZrN, capped with a SiO$_2$ AR layer (Fig. 8g). By precisely optimizing the composition and thickness of each layer using simulation software, the resulting SSAC exhibited exceptional optical properties, achieving a high solar absorptance of 0.965 and a low thermal emittance of 0.086 at 82 °C (Fig. 8h). Importantly, the SSAC maintained high optical performance even after annealing at 600 °C for 10 h, demonstrating excellent thermal stability (Fig. 8i).

In general, dual-ceramic SSACs offer even higher spectral selectivity than simple bilayers because of the more gradual transition in optical properties.[111] Their design, however, is more complex, and fabrication requires careful control to achieve the correct composition and thickness in each layer. Interdiffusion at the interface between the two cermet layers or between the cermet and the substrate can be a concern at high temperatures. Still, with advanced materials like HENs and improved deposition processes, dual-layer graded structures hold great promise. They represent a bridge between simple coatings and more elaborate photonic crystals, capturing some benefits of both approaches.
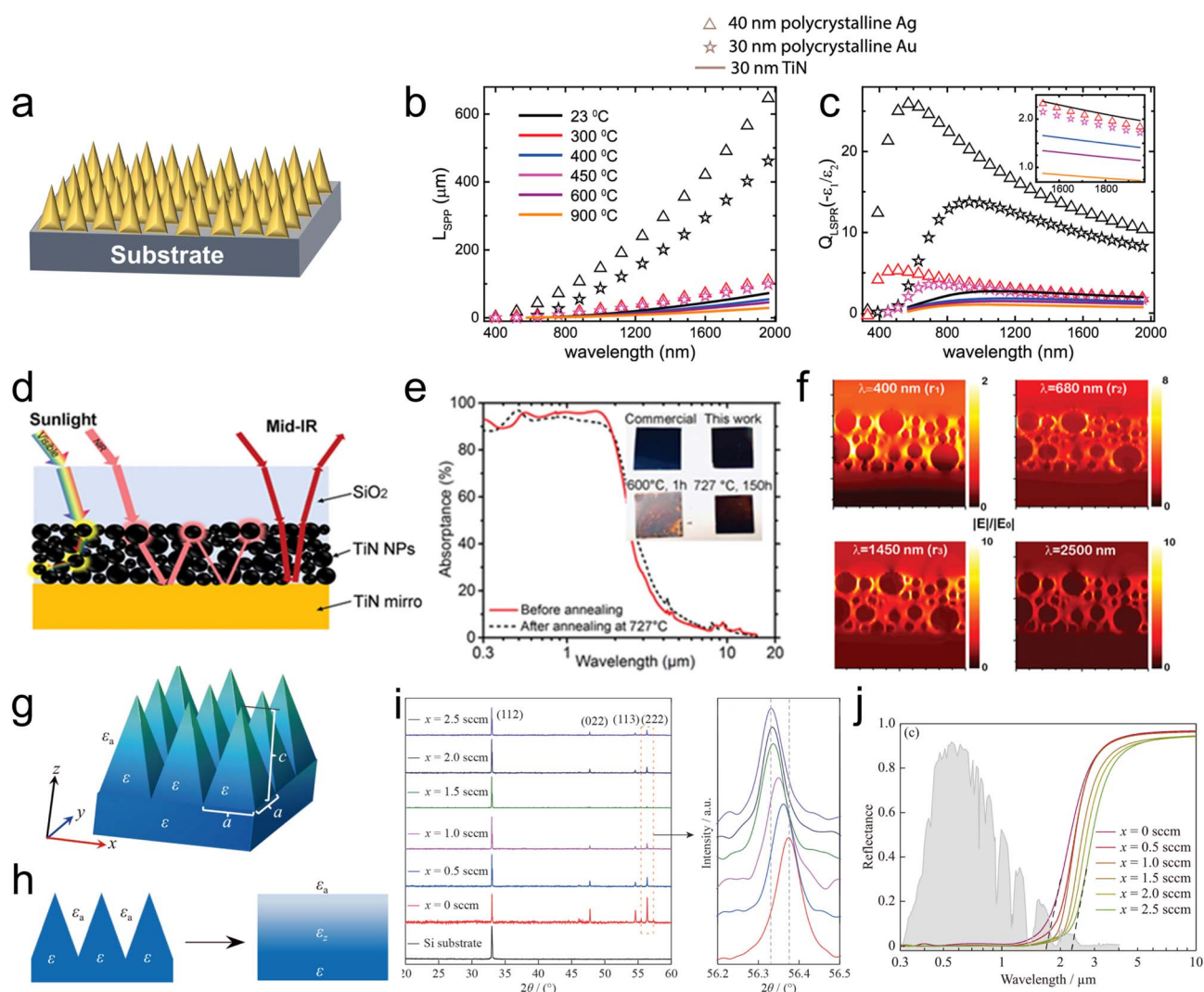

Fig. 9 Fundamentals and advances in plasmonic SSACs. (a) Structural schematic of a plasmonic SSAC. (b) Surface plasmon polariton propagation lengths and (c) localized surface plasmon resonance quality factor for 40 nm Ag, 30 nm Au, and 30 nm TiN at different temperatures.[118] Copyright 2017, American Chemical Society. (d) Schematic of the TiN nanoparticle-based SSAC. (e) Absorptance spectra of TiN nanoparticle-based SSACs before and after annealing. (f) Cross-sectional electric field distributions at different wavelengths.[56] Copyright 2020, Wiley-VCH. (g) Schematic of the NiCuCrFeSiN pyramidal structured hypersurface. (h) Illustration showing the pyramidal structure hypersurface as a layer with a graded dielectric constant (ε). (i) XRD patterns of the Si substrate and NiCuCrFeSiN coating. (j) Simulated reflectance spectra for the NiCuCrFeSiN SSAC.[89] Copyright 2020, Springer Nature.

5.4 Plasmonic and metamaterial SSACs

An alternative route to spectral selectivity leverages nanoscale structuring to manipulate light absorption, rather than using multiple planar layers.[112] Plasmonic SSACs rely on the excitation of localized surface plasmons, which are collective oscillations of electrons in metallic nanostructures, enabling the concentration and trapping of light at specific resonant wavelengths (Fig. 9a). Traditional plasmonic SSACs often used noble metal nanoparticles (like Au or Ag) embedded in a dielectric host to create absorption peaks in the visible range. However, noble metals have drawbacks for solar–thermal applications: they are expensive, have relatively low melting points, and tend to coalesce or oxidize at elevated temperatures, which degrades their optical performance. As a result, there has been a shift toward using refractory plasmonic materials, particularly transition metal nitrides such as TiN, ZrN, TaN, WN, and HfN, which exhibit metallic behavior and plasmon resonance but with far greater thermal stability and durability.[113,114]

TiN, for example, is often touted as a "ceramic gold" because it supports a plasmonic response similar to that of gold while being stable in air up to 800 °C or more.[67,115,116] By incorporating plasmonic nitrides, one can design absorbers that survive conditions where gold- or silver-based nanostructures would fail. For example, Cortie et al.[117] examined TiN nanostructures like thin films and nanoparticle arrays, finding that TiN can support tunable localized surface plasmon resonances from the visible into the near-IR by adjusting particle geometry and the Ti : N stoichiometry. Although TiN's plasmonic quality factor is somewhat lower than that of gold due to higher optical losses in TiN, at elevated temperatures, TiN outperforms gold because Au's properties degrade drastically with temperature, while TiN's remain relatively stable. In fact, Reddy et al.[118] showed that epitaxial TiN films retain their metallic character and plasmonic response up to 900 °C, with only gradual changes in their dielectric function. Above a few hundred degrees, TiN's plasmon resonance becomes comparable in sharpness to Au or Ag, since the noble metals soften and oxidize, whereas TiN does not (Fig. 9b and c). This means TiN and similar nitrides are prime candidates for any application involving high-temperature plasmonics or photothermal conversion.

One challenge with plasmonic absorption is that a single type of nanoparticle or a single resonance typically covers only a narrow portion of the spectrum. To achieve broadband absorption using plasmonics, one can employ either a wide distribution of nanoparticle sizes or a combination of different plasmonic materials and shapes. This, however, can lead to design complexity and sometimes still leaves absorption gaps in the spectrum. Li et al.[56] reported a solution-processed all-ceramic metamaterial absorber composed of a TiN reflective base, a layer of TiN nanoparticles as the absorber medium, and a SiO_2 top layer for AR (Fig. 9d). This structure combined plasmonic absorption with a Fabry–Pérot interference effect, achieving around 95% solar absorptance while keeping thermal emittance as low as ~3%. Crucially, because the entire structure was ceramic, it withstood temperatures up to ~727 °C without significant loss of performance (Fig. 9e and f). Moreover,

Wattoo et al.[88] demonstrated a broadband SSAC by depositing TiAlN via a template- and lithography-free process that naturally produced a vertically aligned conical columnar microstructure. The conical nanostructures create a graded refractive index from air into the film and support multiple internal resonances, leading to very high absorption (0.89) over a broad spectrum. Such nano-columnar nitride coatings combine the benefits of plasmonic absorption with geometric light trapping, and they are inherently durable, thanks to the ceramic nature of TiAlN.

Recently, Wang et al.[89] developed an HEN (NiCuCrFeSi)N for SSACs via RF magnetron sputtering (Fig. 9g and h). The study revealed that the cutoff wavelength of the coating's reflectance spectrum can be intrinsically tuned by varying the nitrogen content during deposition. Uniform composition and homogeneity were confirmed by Rutherford backscattering spectroscopy, while XRD verified the face-centered cubic structure of the films (Fig. 9i). By engineering the nitrogen flow rate, a red shift in the cutoff wavelength was achieved, enabling tailored spectral selectivity for solar absorption and infrared emission. To further enhance performance, a pyramid-structured metasurface was designed, boosting solar absorptance from 0.74 to 0.99 and reducing thermal emittance to as low as 0.06 (Fig. 9j). These results demonstrate the potential of compositional and structural modulation in HEN films for highly efficient, thermally stable, and tunable solar selective absorbing coatings, opening new avenues for advanced photo-thermal conversion technologies.

Nanostructured and plasmonic absorber designs add another toolkit for spectral selectivity. By creating nano-scale patterns or composite structures, one can induce resonant absorption modes that, when properly engineered, overlap to cover the entire solar spectrum. TiN and related compounds shine in this approach by offering the necessary plasma resonance and enduring the high temperatures of solar–thermal operation. Whether through designed metamaterials or self-organized nanostructures, nitride-based absorbers can achieve near-perfect absorption with minimal thickness. Crucially, combining HENs with nanostructuring could further broaden absorption and improve stability, as different constituents may support multiple plasmon resonances and inhibit coarsening of nanostructures.

The thermal stability of coatings in air is critical for CSP applications. As shown in Table 1, several nitride-based coatings exhibit good thermal stability even under air atmospheres. For example, CrO_xN_y/SnO_2 (ref. 73) remains stable after annealing at 278 °C for 600 h in air, $NbAlN/NbAlON/Si_3N_4$ (ref. 77) at 450 °C for 116 h in air, $W/WSiAlN_x/WSiAlOyN_x/SiAlO_x$ (ref. 78) at 450 °C for 400 h in air, W/TiAlN/TiAlSiN/TiAlSiON/ $TiAlSiO_2$ (ref. 80) at 350 °C for 1000 h in air, TiN/TiN nanoparticles/SiO_2 (ref. 56) at 627 °C for 150 h in air, and AlCrMo-TaTiN/Al_2O_3 (ref. 59) at 300 °C for 2 h in air. Although these coatings are relatively thin, they nonetheless demonstrate remarkable thermal stability in air environments.

Despite remarkable progress, several key challenges remain for nitride-based SSACs. Chief among them is the long-standing trade-off between achieving high solar absorptance, maintaining low thermal emittance, and ensuring robust stability at

elevated temperatures and in harsh environments. Conventional coatings often suffer from oxidation, phase segregation, or degradation during long-term operation. HENs, however, offer a compelling pathway to overcome these bottlenecks. Entropy-stabilized single-phase lattices suppress phase separation, while severe lattice distortion and multi-cation electronic states broaden interband transitions, resulting in enhanced broadband absorption and robust high-temperature stability.[4,24] For instance, AlTaTiZrN-based SSACs retained excellent performance after 750 °C for 120 h in a vacuum, with $\alpha \approx 0.933$, $\varepsilon \approx 0.094$ at 82 °C, and $\varepsilon \approx 0.228$ at 750 °C.[24] These findings demonstrate how entropy engineering can simultaneously deliver efficiency and stability, thus providing a pathway toward the next generation of durable and high-performance SSACs.

6 Applications of nitride-based SSACs

The remarkable optical and thermal properties of nitride-based SSACs have opened up a broad array of solar thermal applications. These range from large-scale energy systems, where coatings enable higher efficiency power generation[24,56,80,119–123] to small-scale and emerging technologies like water purification,[124–126] smart textiles,[86,127] and anti-icing surfaces.[90,128,129] In all cases, the combination of high solar absorptance, low thermal emittance, and excellent high-temperature stability that transition metal nitrides and HENs offer is a key enabler.[130] Below, we highlight several major application domains for these coatings, focusing on how nitride SSACs are integrated into devices, their performance metrics, and considerations for durability and scalability.

6.1 High-temperature applications

6.1.1 CSP. In CSP plants, SSACs are crucial for absorbing sunlight on receivers and converting it to heat for electricity generation.[22,131,132] CSP systems, especially for parabolic troughs, use mirrors to focus sunlight onto a receiver, which is often a pipe carrying a heat-transfer fluid (Fig. 10a). Traditionally, commercial CSP receivers have relied on cermet coatings, which are metal–insulator composites and include nitride-based absorbers such as Al_2O_3-W cermets. These coatings provide good spectral selectivity and are effective at operating temperatures up to approximately 400 °C.[22,133] However, when the temperature exceeds approximately 500 °C, traditional SSACs start to degrade due to oxidation, diffusion, or changes in the structure, which cause their emissivity to increase and the overall efficiency to decrease. As next-generation CSP systems aim for operating temperatures of 550 °C or higher to achieve greater Carnot efficiency and support advanced heat-storage media, new absorber materials are needed to meet these demands.

Transition metal nitrides like TiN, CrN, or their alloys can endure higher temperatures than many oxide-based cermets due to their refractory nature and strong bonds.[134] Moreover, as discussed in Section 5, multi-layer nitride/oxynitride coatings can be engineered for superior spectral selectivity. One early

demonstration for CSP was by Cao et al.,[119] who developed a TiN-based multilayer absorber on a $LaAlO_3$ ceramic substrate. The coating consisted of a TiN-SiO_2 cermet layer optimized for solar absorption backed by a reflective tungsten layer and topped with a SiO_2 AR coating. This stack achieved an initial solar absorptance above 95%, and even after annealing at 700 °C it retained about 94% absorptance with only a minor increase in emittance. At the same time, maintaining >90% absorption after exposure to 700 °C was a notable breakthrough, indicating that such nitride-based SSACs could indeed meet the demands of high-temperature CSP plants (Fig. 10b). The study noted that while the optical performance was excellent, considerations such as long-term oxidation needed further optimization. Another approach to CSP absorbers was shown by Barshilia et al.,[80] who developed multi-layer Si-doped nitride/oxide coatings tailored for evacuated receiver tubes. By stacking nanoscale layers of transition-metal nitrides and their oxides, they produced coatings that withstood high vacuum temperatures while delivering the needed absorptance/emittance for CSP (Fig. 10c). Li et al.[56] employed TiN-based all-ceramic plasmonic metamaterial SSACs, which demonstrate a high solar–thermal conversion efficiency (89%) for high-temperature operation (Fig. 10d). Thermal stability tests show the absorber maintains high performance after 150 h of annealing at 727 °C in a vacuum and up to 627 °C in air, indicating excellent durability. Outdoor and indoor tests confirm its effectiveness in raising temperatures for practical photothermal applications, outperforming commercial selective and nonselective absorbers (Fig. 10e). This plasmonic metamaterial absorber offers a universal, cost-effective platform for CSP systems.

The introduction of HENs has shown exceptional thermal stability enhancement for CSP plants. Zhao et al.[24] developed HEN-based SSACs specifically, which consisted of a bilayer structure, including an AlTaTiZrN HEN layer and a Si_3N_4 AR layer, fabricated via magnetron sputtering. High-entropy engineering enables a complex and intensified electronic band structure, significantly enhancing solar absorption via increased 3d interband transitions. The absorber demonstrates outstanding spectral selectivity and exceptional thermal robustness, maintaining high optical performance ($\alpha = 93.3\%$ and $\varepsilon_{82 °C} = 9.4\%$) even after 120 h of annealing at 750 °C in a vacuum. Photothermal testing shows rapid and high equilibrium temperature rise and excellent temperature gains when integrated in vacuum collector tubes, outperforming nonselective absorbers both under laboratory and outdoor conditions. Simulations and field tests confirm superior photothermal conversion efficiency (up to 57.44% at 750 °C and 100 suns) and significant liquid temperature retention day and night, even under real-world conditions (Fig. 10f–i). For comparison, most conventional coatings would have completely oxidized or spalled by that point. Such results strongly suggest that HEN coatings are prime candidates for next-generation CSP plants aiming at 700 °C or above.

In summary, nitride-based SSACs in CSP plants serve to increase the amount of solar heat captured and decrease losses, especially as the field moves to higher temperature regimes.[135] By using advanced architecture and materials, researchers have
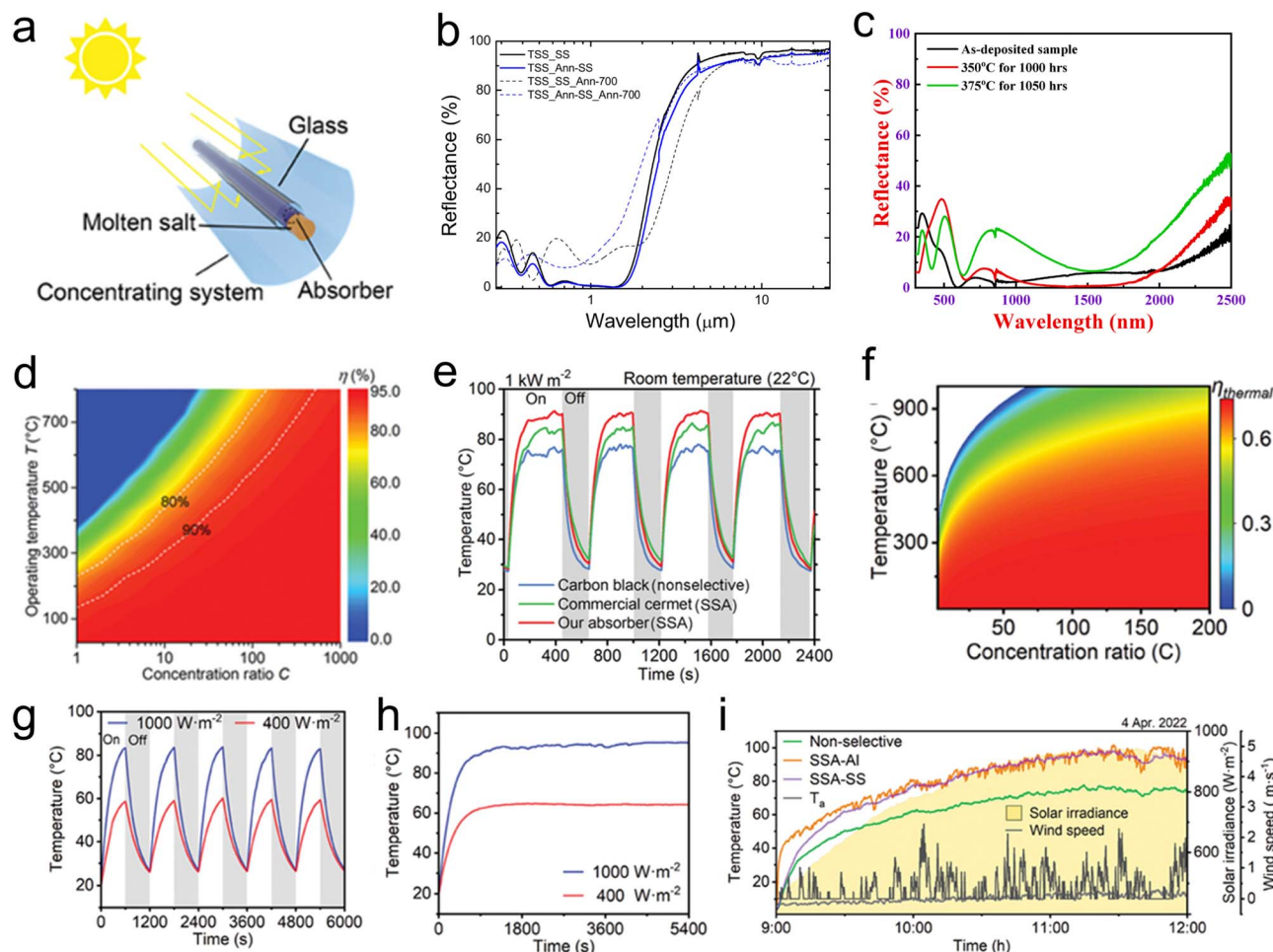
Fig. 10 Applications of SSACs in CSP systems. (a) Schematic of a parabolic trough collector system.[24] Copyright 2024, Wiley-VCH. (b) Reflectance spectra of the TiN–SiO$_2$-based SSAC before and after annealing.[119] Copyright 2016, Elsevier. (c) Reflectance spectra of the W/TiAlN/TiAlSiN/TiAlSiON/TiAlSiO SSAC before and after annealing in air at 350 °C for 1000 h and 375 °C for 1050 h.[80] Copyright 2022, Elsevier. (d) Photothermal conversion efficiency of the TiN nanoparticle-based SSAC. (e) Temperature change under 1 sun irradiation.[56] Copyright 2020, Wiley-VCH. (f) Photothermal conversion efficiency of the AlTaTiZrN-based SSAC. (g) Cyclic and (h) long-term testing indoors under different light conditions; (i) outdoor test results.[24] Copyright 2024, Wiley-VCH.

extended the viable operating range of SSACs from the traditional ∼500 °C limit to 600 °C, 700 °C and beyond. These coatings ensure that more of the concentrated sunlight is converted to heat and that the heat is retained by the receiver, thereby improving the overall thermal efficiency of the plant. As the CSP technology evolves, for instance, incorporating thermal energy storage or new high-temperature working fluids, the importance of stable selective coatings only grows. It is likely that entropy-engineered nitride coatings and similar innovations will become key enabling materials for the next-generation CSP systems.

6.1.2 Solar thermoelectric generators. Another high-temperature application of SSACs is in solar thermoelectric generators (STEGs).[136] An STEG is a solid-state device that converts solar heat directly into electricity using thermoelectric modules. It consists of a solar absorber that heats up and creates a temperature difference across thermoelectric legs; the thermoelectric materials then generate electrical power *via* the

Seebeck effect. The efficiency of an STEG depends critically on how hot the absorber can get relative to the cold side and how well it can maintain that temperature difference. Here, SSACs are indispensable as the interface capturing sunlight: they need to absorb sunlight efficiently to drive the hot-side temperature up but also not lose too much heat by radiation or convection.

SSACs have proven highly beneficial for STEGs because of their ability to withstand high temperatures and harsh conditions and because they can be directly integrated into the surfaces of thermoelectric modules or heat spreaders. For example, Kraemer *et al.*[120] successfully implemented a commercial SSAC in a flat-panel STEG design featuring nanostructured Bi$_2$Te$_3$ thermoelectric legs enclosed within a vacuum chamber to eliminate convective losses (Fig. 11a). Utilizing a thermal concentration strategy, their design ensured a large absorber area relative to the smaller cross-sectional area of the thermoelectric legs, significantly enhancing the temperature gradient. Consequently, this configuration achieved
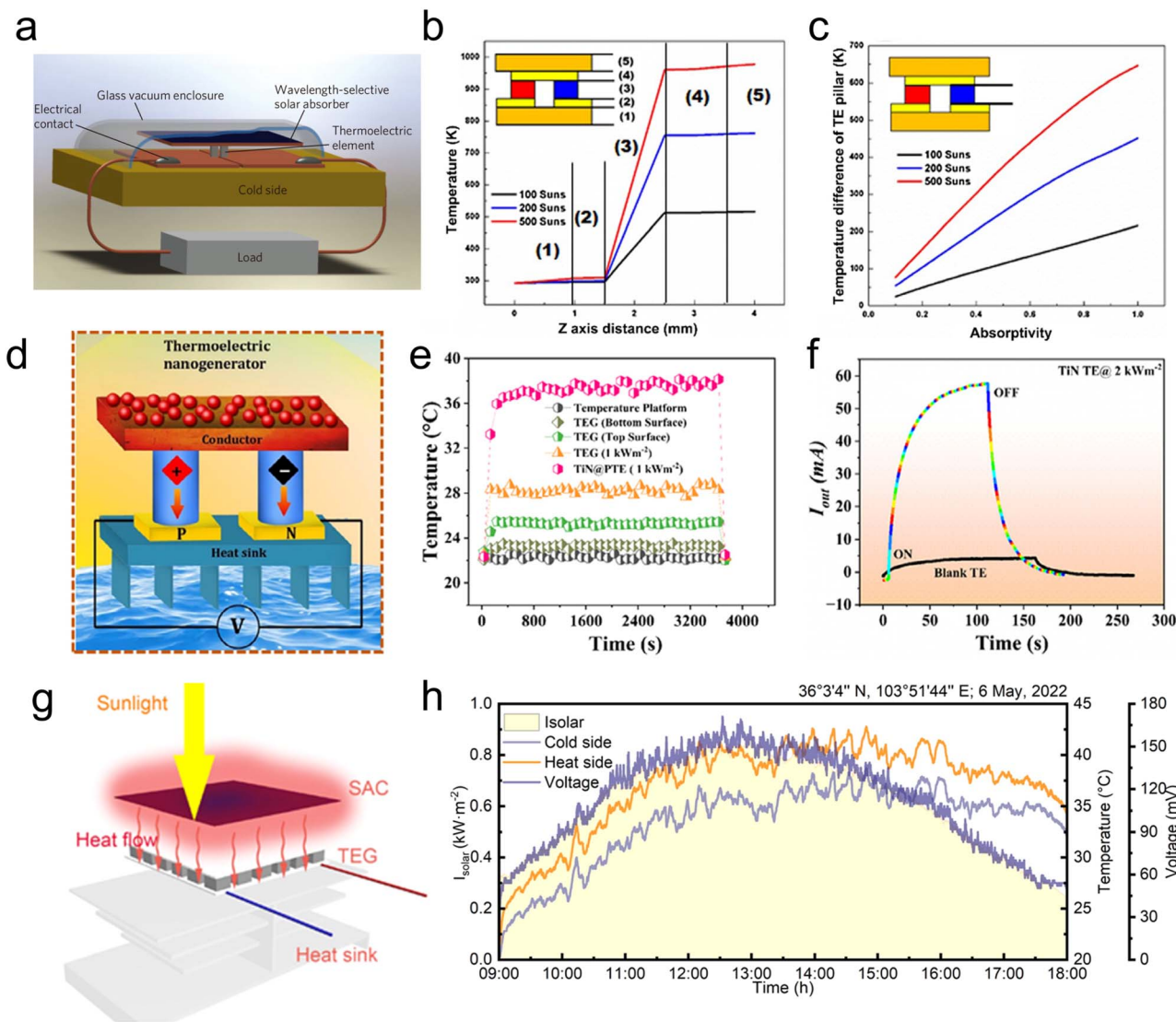
Fig. 11 Applications of SSACs in STEGs. (a) Schematic of an STEG cell.[120] Copyright 2011, Springer Nature. (b) Temperature variations in different regions of the STEG under different light conditions. (c) Temperature difference between the top and bottom of TE columns as a function of absorptivity under different light illumination.[121] Copyright 2018, Elsevier. (d) Schematic of the TiN-based PTE placed over a fin radiator. (e) Temperature change at 1 kW m^{-2} for 1 h. (f) Time-dependent open-circuit current measurement under 2 kW m^{-2}.[122] Copyright 2023, Wiley-VCH. (g) Schematic of an STEG assisted by HEN SSACs; (h) outdoor test of the STEG.[123] Copyright 2022, American Chemical Society.

a solar-to-electric efficiency of 4.6–5.2% under standard one sun illumination (AM1.5), marking a substantial improvement over previous flat-panel STEG efficiencies.

Further innovations are illustrated by Jiang *et al.*,[121] who developed a two-dimensional TiN photonic crystal absorber with exceptional broadband absorption and suppressed infrared emissivity (Fig. 11b and c). Notably, this photonic structure demonstrated robust thermal stability, maintaining its optical properties even after high-temperature annealing above 1000 K. When integrated into STEGs, this absorber elevated hot-side temperatures by approximately 30 K more than conventional black coatings under identical illumination, substantially enhancing thermoelectric voltage and power output. Candadai *et al.*[137] adopted an alternative approach, employing multilayer tungsten and nitride ceramic SSACs

paired with standard Bi$_2$Te$_3$ thermoelectric modules. Their multilayer absorber, composed of alternating layers of W, TiAlN, and TiAlSiN, achieved high absorptance (∼95.6%) and low emittance (∼7%) at elevated temperatures (∼82 °C). Under concentrated illumination (62 suns), the absorber reached ∼512 °C, enabling the system to achieve a practical conversion efficiency of around 1.2%, demonstrating the potential of integrating commercial thermoelectric modules with advanced nitride-based coatings.

Addressing scalability and ease of manufacturing, Almutairi *et al.*[122] utilized TiN nanoparticle-based paintable absorbers, achieving a solar absorptance of 92.5%. Under modest illumination (1–2 suns), these coatings rapidly heated, producing measurable electrical output from integrated thermoelectric generators, demonstrating practical photothermal-to-electric

conversion potential in scalable applications (Fig. 11d–f). Pushing the thermoelectric performance further, Kraemer et al.[138] also explored concentrating STEGs utilizing segmented thermoelectric legs under extreme solar concentration over 200 kW m^{-2}, achieving absorber temperatures near 600 °C and overall system efficiencies up to 9.6%. Similarly, Cheruvu et al.[139] demonstrated real-world viability through a multilayer nitride absorber (TiAlN/TiAlSiN/TiAlSiON) coated on stainless steel. Operating under vacuum with concentrated sunlight, their STEG reached a hot-side temperature of 470 °C, delivering ~0.91 W power with a notable efficiency of ~2.2%.

Recently, Liu et al.[123] explored HEN-based absorbers integrated with STEGs, achieving remarkable spectral selectivity with a solar absorptance of ~95.2% and a thermal emittance of ~10.9% (Fig. 11g). Under standard illumination, their device effectively elevated surface temperatures and generated measurable power, showcasing the potential for advanced entropy-stabilized nitrides to drive future STEG advancements (Fig. 11h). Overall, nitride-based SSACs are pivotal in enhancing STEG performance, ensuring high operational temperatures, durability, and compatibility with emerging thermoelectric technologies. Continued development and integration of these advanced SSACs will likely remain a critical pathway toward achieving practical, high-efficiency solar thermoelectric power generation systems.

6.2 Low-temperature and emerging applications

Not all uses of photothermal coatings involve extreme temperatures; there are many applications at moderate or low temperatures where solar absorbers are used to drive useful effects. Low-temperature in this context is relative, and often these applications involve direct heat utilization rather than electricity generation. Nitride-based SSACs are increasingly finding roles here as well, owing to their broadband absorption and durability in various environments. We will discuss a few notable areas: solar-driven water evaporation/desalination,[11,140] personal thermal management,[141] and passive anti-icing surfaces. In each case, SSACs can enhance performance, though the emphasis may differ.

6.2.1 Solar-driven water evaporation. Solar-driven evaporation has emerged as a promising route for desalination and water purification, leveraging photothermal materials to localize heat at the water–air interface and significantly enhance evaporation rates.[142] Effective systems prioritize intense localized heating with minimal heat loss to bulk water, leading to innovative designs such as floating absorbers and porous membranes. Among the various photothermal materials explored, nitride-based SSACs stand out due to their exceptional broadband absorption and robustness in harsh, saline, and wet environments.

Pioneering work by Chen et al.[143] first demonstrated SSAC utility in interfacial evaporation, where a floating receiver efficiently localized solar heat at the water surface, achieving steam generation at 100 °C under standard solar illumination (1 sun). The employed commercial SSAC exhibited high solar absorptance ($\alpha \approx 0.93$) and low thermal emittance ($\varepsilon \approx 0.07$),

dramatically reducing radiative and convective losses. Building upon these foundational results, subsequent studies have further optimized nitride-based SSAC structures to enhance evaporation performance. For example, He et al.[87] developed a three-layer HEN MoTaTiCrN-based SSACs, comprising layers of high-metal content for absorption, low-metal content for extinction, and an anti-reflection Si$_3$N$_4$ topcoat. This advanced design yielded superior optical performance ($\alpha \approx 95.2\%$; $\varepsilon \approx 6.8\%$), affirming the effectiveness of multi-layer engineering to enhance both the evaporation efficiency and scalability.

To optimize interfacial heating further, Chang et al.[124] designed a three-dimensional porous evaporator integrating a TiNO$_x$-based SSAC with porous copper foam (Fig. 12a and b). This architecture significantly amplified the evaporation efficiency under low solar flux conditions (1 sun), achieving an exceptional solar-to-steam conversion efficiency of ~48%. The strategic combination of broad solar absorption (~0.95), minimal thermal emission (~0.05), and efficient thermal localization through hydrophilic–hydrophobic interfaces underscores the value of tailored porous structures in enhancing evaporation performance (Fig. 12c).

Despite these advancements, practical challenges such as salt accumulation and fouling remain critical barriers in long-term operation. Bian et al.[125] addressed this by developing a solar thermal vapor generator (STPV) with a commercial TiNOx SSAC ($\alpha \approx 0.92$; $\varepsilon \approx 0.04$). Utilizing a floating design and an absorbent paper substrate, the device formed a wet, porous salt layer instead of dense salt deposits (Fig. 12d–f). This porous structure enabled continuous vapor permeation and sustained evaporation rates under severe fouling conditions, markedly outperforming conventional solar evaporators. Extending the functionality of SSACs, Menon et al.[126] introduced a passive, non-contact "solar umbrella" design, incorporating a TiNO$_x$ absorber and a blackbody emitter to radiatively transfer localized heat directly to the water surface (Fig. 12g). This innovative strategy nearly doubled the evaporation efficiency compared to traditional systems, significantly reducing the spatial footprint required for zero-liquid-discharge wastewater management (Fig. 12h and i).

Moreover, Wang et al.[144] advanced the application further by coupling photovoltaic and membrane distillation technologies in an integrated photovoltaic membrane distillation (PVMD) system. Here, the SSAC-equipped photovoltaic module efficiently converted sunlight into thermal energy, which was sequentially reused across multiple distillation stages, achieving impressive fresh water production rates up to 3.25 kg m^{-2} h^{-1} alongside high electricity generation efficiency (>11%). This integrative strategy exemplifies the potential for multifunctional devices to concurrently address energy and water demands sustainably. Collectively, through strategic integration of photothermal materials, structural optimization, and innovative thermal management approaches, recent research is effectively addressing both efficiency and practical operational challenges. As water scarcity intensifies globally, continued advancements in robust, scalable, and highly efficient solar evaporation technologies hold great promise for sustainable
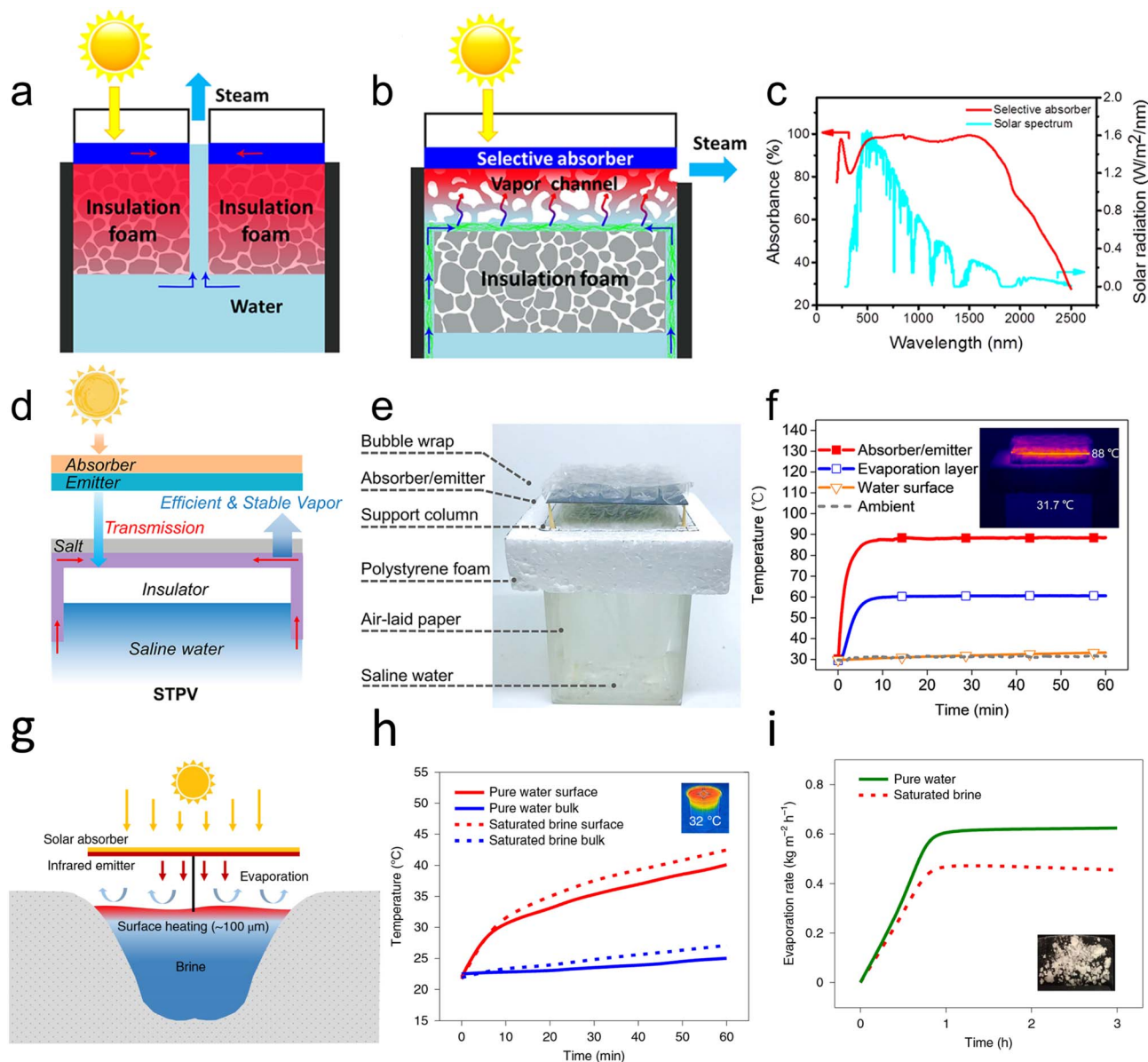
Fig. 12 Applications of SSACs in solar-driven water evaporation. (a) Schematic of a thermally concentrated interfacial evaporator; (b) schematic structure of a 3D porous interfacial evaporator; (c) absorption spectrum of $TiNO_x$-based SSACs.[124] Copyright 2019, American Chemical Society. (d) Schematic and (e) photograph of a solar-driven evaporator; (f) temperature change curves as a function of irradiation time.[125] Copyright 2021, American Chemical Society. (g) Mechanistic diagram of the solar umbrella; (h) surface and bulk temperature changes over 1 h with the solar umbrella; (i) evaporation rate over a 3 h period with the solar umbrella.[126] Copyright 2020, Springer Nature.

water purification solutions at various scales, from personal use to community-wide implementations.

6.2.2 Personal thermal management. Controlling thermal comfort for individuals, for example, keeping someone warm on a cold day under intense sun, can also benefit from SSACs.[86] Traditional clothing provides insulation, but it does not actively make use of solar radiation or radiative heat exchange in a controlled way. By incorporating an SSAC into textiles, one can design smart garments that either absorb sunlight to warm the body. Nitride-based SSACs are attractive here because they can be made into very thin, flexible films or nanoparticles that provide the desired optical properties without making the fabric

stiff or heavy.[145] They are also stable to outdoor conditions and washing, which is obviously critical for any wearable application.

A fascinating example is a nitride-coated textile that not only provided passive heating but also generated electricity from motion. In this demonstration, Zhang *et al.*[127] created a tri-layer fabric comprising (1) a TiN nanoparticle-based layer that has high solar absorptance (~83.7%) but low mid-IR emissivity (~11%), (2) a conductive layer of copper/nickel-coated textile for distributing heat and also serving as an electrode for energy harvesting, and (3) a PTFE nanofiber membrane that acted as a triboelectric generator layer (Fig. 13a and b). The TiN based
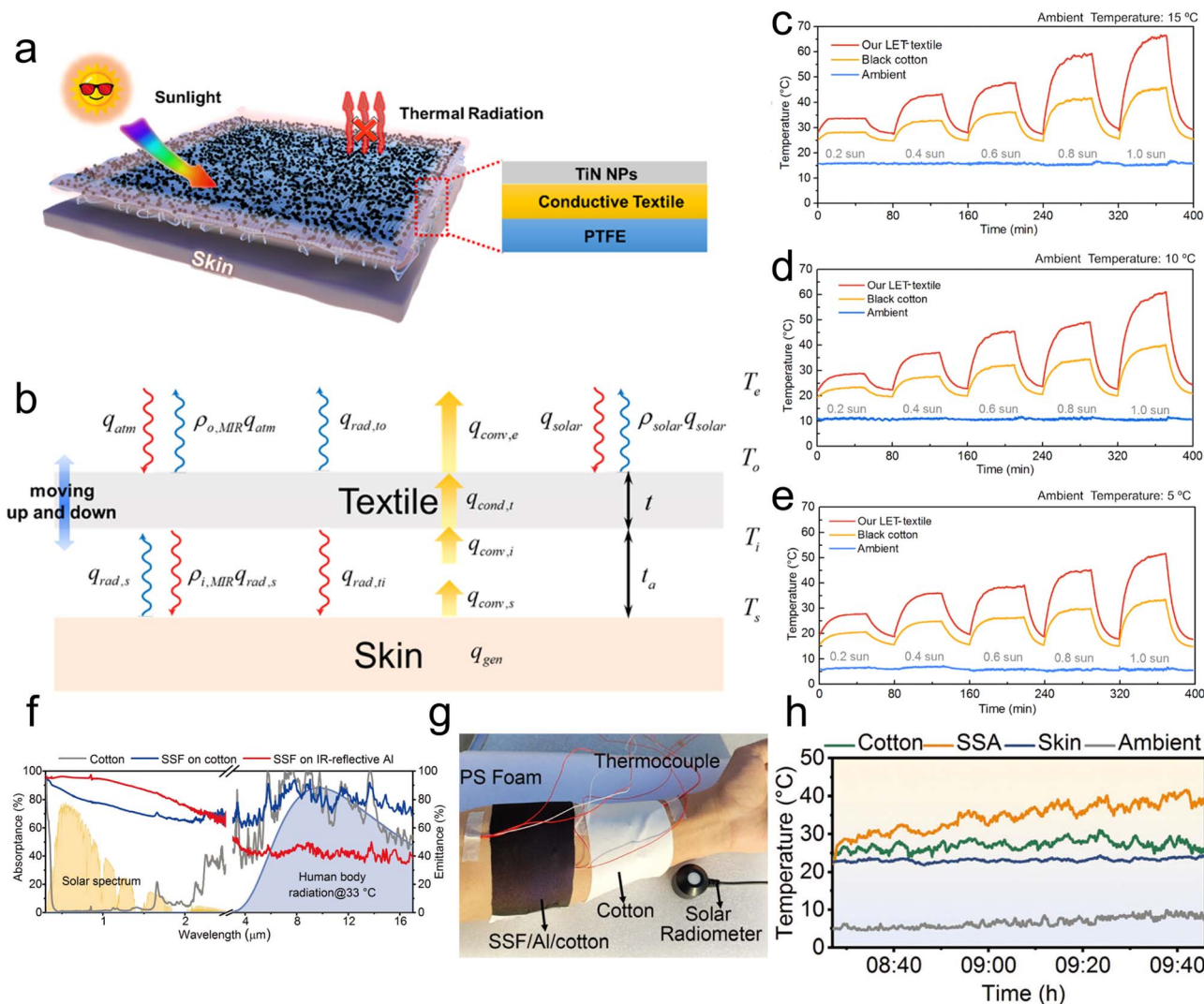
Fig. 13 Applications of SSACs in personal thermal management. (a) Schematic structure of TiN-based spectrally selective fabrics. (b) Schematic of the heat transfer model. (c–e) Skin temperature changes of TiN-based spectrally selective fabrics and black cotton cloth at ambient temperatures of 15 °C, 10 °C, and 5 °C.[127] Copyright 2022, Elsevier. (f) Absorption spectra of ZrNbMo-Al-N-based spectrally selective fabrics. (g) Photograph of an outdoor test. (h) Temperature changes recorded during outdoor tests on a human subject.[86] Copyright 2022, Wiley-VCH.

SSAC has low emissivity in the IR, which helps retain heat so that once it absorbs sunlight, it does not re-radiate much of it away, thereby warming the wearer more effectively. Under sunlight, this TiN-based textile can warm up significantly, allowing someone to feel warmer or potentially reduce indoor heating needs (Fig. 13c and d). Indeed, tests showed that wearing this solar-absorbing textile could allow building thermostats to be turned down by a few degrees (around 3 °C) while maintaining comfort, which could translate into substantial energy savings. At the same time, the inclusion of a triboelectric nanogenerator means the fabric can also convert mechanical motion into electricity. Moreover, the textile remained lightweight, breathable, and could be washed, indicating that adding the TiN and metallic layers did not ruin its wearability.

For warming applications, one could also consider the HEN-based SSAC. He et al.[86] demonstrated the use of magnetron sputtering to apply a graded-index multilayer coating

containing an HEN onto a cotton fabric. They achieved extremely high solar absorptance (~92.8%) and relatively low infrared emittance (~39.2%) on the fabric (Fig. 13f). In practical terms, under a cold ambient (0 °C) with moderate sun (600 W m^{-2}, roughly 0.6 sun), the coated fabric reached a photothermal conversion efficiency of 82%, meaning it was very effective at converting that sunlight to heat on the body. Even under weaker sunlight (350 W m^{-2}) and 7.5 °C ambient, it could raise the temperature of a simulated skin surface by 12 °C, which can be the difference between discomfort and comfort on a chilly day (Fig. 13g and h). What is notable is that they achieved this without significantly compromising the textile's feel: the sputtered coating was engineered to be thin and conformal enough to preserve the fabric's porosity and flexibility. A major hurdle for applying inorganic coatings to fabrics is adhesion and durability. In the HEN multilayer adhered strongly to each fiber and did not crack under bending; it also survived at least 10

laundry cycles with negligible change in optical performance. By not clogging the pores of the cotton, the coating preserved breathability, which is a crucial aspect so that wearing the fabric does not become uncomfortable or lead to sweat build up.

In summary, nitride-coated textiles demonstrate how spectrally selective concepts can translate into the wearable scale. Photothermal clothing that harvests sunlight to keep warm or conversely reflects sunlight to keep cool represents an innovative intersection of energy technology and apparel.[146] The use of materials like TiN and HENs ensures that these coatings can endure everyday wear and weather exposure.

6.2.3 Photothermal anti-icing and de-icing. In cold regions, ice accumulation on surfaces (power lines, wind turbine blades, airplane wings, roads, *etc.*) is a serious problem, causing safety

hazards and efficiency losses.[147,148] Current anti-icing methods often involve energy-intensive heating (like resistive heaters) or chemical de-icers (like salts or glycols) that have environmental downsides.[149–151] SSACs offer a passive or minimally powered solution: under sunlight, a photothermal surface can heat up and either prevent ice from forming or help melt it off. To be effective, such a coating usually should also be superhydrophobic so that water droplets have a harder time sticking and forming ice in the first place, and any melted water easily rolls off. This combination of a solar absorber with a water-repellent texture gives dual protection: delay ice nucleation and actively heat the surface to melt any frost or ice that does form when the Sun comes out.
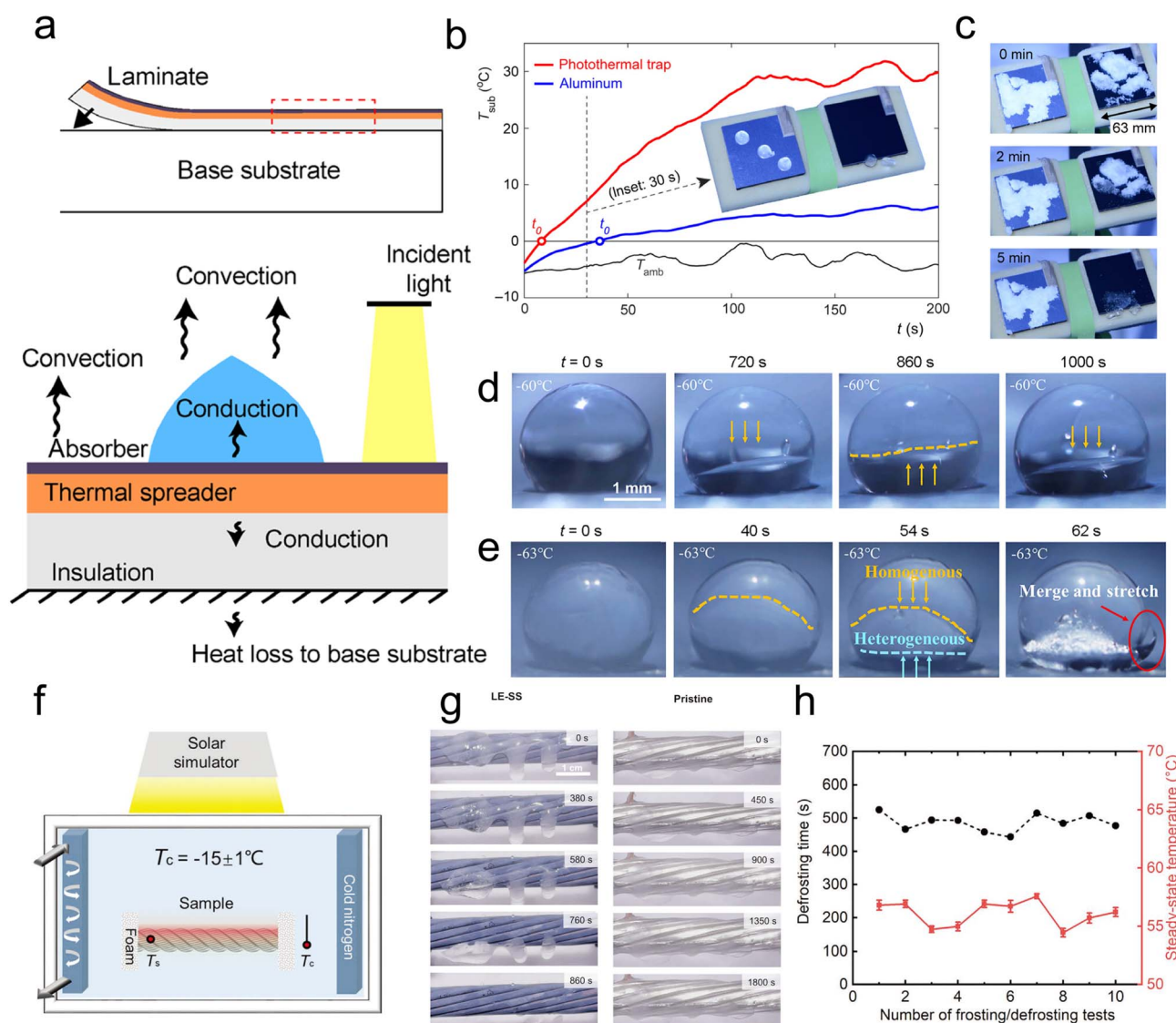

Fig. 14 Applications of SSACs in photothermal anti-icing and de-icing. (a) Schematic of a photothermal trap. (b) Temperature rise during light exposure, resulting in 0.5 ml frozen droplets sliding off. (c) Snow melting on a photothermal surface.[128] Copyright 2018, The American Association for the Advancement of Science. (d and e) Droplet freezing experiments performed by adjusting the room temperature to set points and maintaining at 60 °C and 63 °C, respectively.[129] Copyright 2021, Cell. (f) Schematic of the deicing experiment setup. (g) Comparison of the deicing effect of cables coated with titanium nitride and cables not coated with TiN-based SSACs. (h) Defrost time for 10 frost/defrost cycles of TiN-based SSAC-coated cables and 1 sun steady-state surface temperature measured after each cycle.[90] Copyright 2022, Wiley-VCH.

Dash et al.[128] developed a scalable photothermal trap laminate, consisting of an SSAC, a thermal spreader, and an insulation layer, to efficiently remove ice under solar illumination (Fig. 14a). The SSAC exhibits high solar absorptance (~95%) and low thermal emittance (~3%), enabling strong photothermal conversion and minimal radiative loss. Upon illumination, heat is efficiently confined and laterally spread at the ice–substrate interface, rapidly raising the surface temperature and forming a thin lubricating melt layer that enables fast and energy-efficient removal of ice, frost, or snow (Fig. 14b). Laboratory and outdoor tests demonstrated that the photothermal trap enables prompt ice melting and sliding, even at very low ambient temperatures (down to − 25 °C) and under weak sunlight (Fig. 14c). Compared to conventional metal or insulating substrates, only the SSAC-based laminate provided sufficient surface heating for rapid deicing. The approach is robust under inhomogeneous illumination and can be scaled to large surface areas for applications such as wind turbines, power lines, and solar panels.

Ma et al.[129] designed a superhydrophobic SSAC by embedding plasmonic TiN nanoparticles in a hierarchical micro-/nanostructured surface on aluminum. This structure combines high solar absorptance (~90%) with low mid-infrared emittance, enabling outstanding photothermal conversion and significantly reducing radiative heat loss. Under 1 sun illumination, the SSAC achieves rapid temperature increases and exceptional anti-icing performance, preventing droplet freezing even at ~60 °C, far surpassing conventional black or nonselective absorbers (Fig. 14d and e). The synergy between superhydrophobicity and spectral selectivity gives the SSAC durable icephobicity, rapid deicing, and defrosting with minimal energy input, maintaining performance through repeated cycles. Fabricated via a scalable, low-cost solution-based process, the SHSSA offers practical and sustainable anti-icing/deicing for applications in extreme cold environments, outperforming traditional approaches in efficiency and durability.

Li et al.[90] developed a spray-coated, solar-assisted superhydrophobic nanocoating for overhead power lines, combining a plasmonic TiN-based SSAC with dual-scale silica particles for robust water repellency. The absorber exhibits high solar absorptance (90%) and low mid-infrared emissivity (6%), enabling strong photothermal conversion while minimizing radiative heat loss. This coating maintains excellent superhydrophobicity (water contact angle: ~173°) even at low temperatures (down to −15 °C), ensuring both passive anti-icing and rapid active deicing/defrosting. Under simulated 1 sun irradiation at −15 °C, the coated power lines achieved rapid ice melting and removal within 860 s, while uncoated cables remained fully frozen (Fig. 14f and g). The photothermal effect of TiN SSAC quickly raises the cable temperature, melting the ice at the interface; combined with superhydrophobicity, this enables the ice shell to slide off cleanly and keeps the surface dry. The coating also demonstrated excellent durability, retaining deicing and anti-frosting performance after multiple cycles (Fig. 14h), and is compatible with both flat and complex curved surfaces, making it highly practical for real-world deicing of power infrastructure.

In all these cases, nitride-based photothermal coatings provide a passive or solar-assisted way to combat ice, harnessing sunlight to do the work.[152,153] They are essentially self-heating surfaces when the sun is out. Because they rely on sunlight, they are most effective in daytime icing scenarios or to remove frost in the morning, etc. For nighttime, some could be combined with thermal storage like the phase change material or just serve as a superhydrophobic passive surface. Importantly, unlike conventional black paints, these coatings are engineered to maximize solar absorption and to minimize heat losses. Moreover, since materials like TiN are UV-stable and mechanically robust, these surfaces should have a long service life outdoors.[154] This contrasts with some polymeric superhydrophobic coatings that might UV-degrade or wear off quickly. In essence, photothermal anti-icing coatings merge surface chemistry (hydrophobicity) with solar–thermal engineering.[155] By keeping surfaces dry and actively melting frost/ice, they can greatly reduce the frequency of deicing operations or the need for external energy[156,157] and show promising use on wind turbine blades and aircraft exteriors.[158]

7 Conclusion

In this review, we discussed the mechanisms, including plasmonic effects, tailored electronic transitions, defect-mediated absorption, and entropy-driven stabilization, which enable these advanced performance levels. We also reviewed the state-of-the-art fabrication methods, from magnetron sputtering and CVD to solution processing, which have been instrumental in producing both classical and HEN coatings. Furthermore, various design strategies, such as multilayer structures, compositional grading, and nanostructured metamaterials were analyzed, illustrating how the combination of material innovation and structural engineering has led to absorber coatings that approach the theoretical idea of perfect selectivity. The wide array of applications we surveyed, spanning high-temperature CSP receivers, STEGs, solar water desalination, personal thermal textiles, and anti-icing surfaces, underscores the versatility and impact of nitride-based SSACs. In each domain, nitrides, especially when augmented by entropy engineering or nanoscale structuring, provide a unique blend of high performance and robustness, enabling technologies to reach capabilities that would be difficult or impossible otherwise.

Despite these successes, important challenges and opportunities lie ahead. Fundamentally, there is a need for deeper understanding of HENs: how exactly do their complex compositions and atomic-scale disorder influence charge transport, light absorption across different wavelengths, and durability under long-term solar cycling? Answering these questions will likely require advanced computational modeling as well as high-throughput experimental studies to map composition–property relationships across the vast compositional space of HENs. Such efforts could accelerate the discovery of optimal alloy combinations. For instance, identifying which five or six-element nitride yields the best performance for a given application like a CSP absorber or solar-powered water purifier.

On the engineering side, economically scaling up HEN coatings remains a critical hurdle. Magnetron sputtering, as the most widely used PVD method for SSACs, offers strong adhesion between the coating and substrate, dense and pure micro-structures, excellent film uniformity, scalability to large areas, and environmentally benign processing.[159–161] However, conventional multi-target co-sputtering, while effective for compositional control, inevitably increases process complexity and cost. To overcome this, a self-doping reactive sputtering strategy has been proposed. In this process, a single metal target is sputtered in a controlled atmosphere where the reactive gas (O_2 and N_2) flow is much lower than that of the sputtering gas (Ar). Only a limited number of reactive ions interact with the target atoms, producing non-stoichiometric metal compounds. Metal nanoparticles embedded in a ceramic dielectric matrix are thereby formed, and by adjusting the Ar/reactive gas ratio, the composition of the metal–ceramic composite can be finely tuned, enabling transitions from metallic to intermediate or dielectric states. This approach enables fabrication of self-doped, metal–ceramic SSACs with a single target, simplifying production and reducing costs.

Based on this concept, an industrial-scale continuous magnetron sputtering model has been proposed for large-volume production of SSACs on vacuum receiver tubes.[10] Using multiple independent vacuum chambers, successive layers can be deposited without interrupting the vacuum environment, enabling continuous and efficient fabrication. Moreover, self-doping sputtering is applicable to large-area coatings on metal foil via roll-to-roll or air-to-air deposition lines.[10] Among these, air-to-air production lines offer significantly higher throughput and better quality control, though high equipment costs remain a barrier to widespread adoption.

In addition to PVD and CVD techniques, solution-based bottom-up fabrication strategies are emerging as promising alternatives for the large-scale preparation of HEN-based SSACs. Methods such as sol–gel processing, wet-chemical synthesis, and spray coating provide significant advantages in terms of low cost, high throughput, and compatibility with flexible or complex substrates. These features make solution processing highly attractive for practical applications that require scalable and economical manufacturing. Nevertheless, challenges such as precise stoichiometry control, achieving dense microstructures, and ensuring long-term thermal stability, especially in high-temperature and oxidative environments, must be carefully addressed. Future efforts to resolve these issues could establish solution-based processes as a revolutionary pathway for next-generation HEN coatings.

Another promising direction is the hybridization of entropy-engineered materials with micro-/nanostructural design. We have seen initial examples where HENs serve as the absorbing medium in a metamaterial structure. There is fertile ground for designing hybrids that exploit both the intrinsic merits of HENs and the extrinsic enhancements of photonic structures. Such hybrids could yield absorbers that are not only selective and extremely stable but also tunable or multifunctional. Imagine a coating that can switch its spectral properties on demand, or that simultaneously acts as a selective absorber and a catalytic surface for chemical reactions, or as a sensor that can withstand high temperatures. High-entropy materials, with their tendency to form stable, single-phase solutions, could offer a platform for these multifunctional coatings by accommodating dopants or secondary phases without losing structural integrity.

Finally, translating these advanced coatings into real-world systems will benefit from interdisciplinary collaboration. Materials scientists can invent and refine the coatings, but input from system engineers is crucial to define practical requirements. For example, what exact wavelength range needs suppressed emission for a thermophotovoltaic system, or how a coating interacts with a particular heat transfer fluid in a CSP plant. Conversely, breakthroughs at the material level can inspire new system architecture, allowing a solar reactor to operate hotter or a wearable device to generate electricity from the Sun. By working together, researchers and engineers can ensure that the next-generation of SSACs not only excel in the lab but also deliver tangible improvements in efficiency, durability, and functionality in the field.

Conflicts of interest

There are no conflicts to declare.

Data availability

No primary research results, software or code have been included and no new data were generated or analysed as part of this review.

Acknowledgements

References

1 Y. Zhu, Z. Tang, L. Yuan, B. Li, Z. Shao and W. Guo, *Chem. Soc. Rev.*, 2025, **54**, 1027–1092.
2 X. Cui, Q. Ruan, X. Zhuo, X. Xia, J. Hu, R. Fu, Y. Li, J. Wang and H. Xu, *Chem. Rev.*, 2023, **123**, 6891–6952.
3 S. Shi, P. Lv, C. Valenzuela, B. Li, Y. Liu, L. Wang and W. Feng, *Small*, 2023, **19**, 2301957.
4 C.-Y. He, Y. Li, Z.-H. Zhou, B.-H. Liu and X.-H. Gao, *Adv. Mater.*, 2024, **36**, 2400920.
5 B. Liu, C. He, Y. Li, Z. Li, W. Wang, Z. Lu, Z. Wang, S. Zhao, G. Liu and X. Gao, *Matter*, 2024, **7**, 140–157.
6 L. A. Weinstein, J. Loomis, B. Bhatia, D. M. Bierman, E. N. Wang and G. Chen, *Chem. Rev.*, 2015, **115**, 12797–12838.
7 K. P. Sibin and R. Pitchumani, *Renewable Sustainable Energy Rev.*, 2025, **207**, 114959.
8 K. K. Phani Kumar, S. R. Atchuta, M. Shiva Prasad, H. C. Barshilia and S. Sakthivel, *Sol. Energy Mater. Sol. Cells*, 2024, **277**, 113080.

9 Z. Wu, J. Wang, Y. Liu, S. Hou, X. Liu, Q. Zhang and F. Cao, *Mater. Today Phys.*, 2021, **18**, 100388.

10 C. Wang, W. Li, Z. Li and B. Fang, *Renewable Sustainable Energy Rev.*, 2020, **134**, 110277.

11 Y. Li, C. Lin, J. Huang, C. Chi and B. Huang, *Glob. Chall.*, 2021, **5**, 2000058.

12 B. Yang, C. Li, Z. Wang and Q. Dai, *Adv. Mater.*, 2022, **34**, 2107351.

13 Z.-H. Zhou, C.-Y. He and X.-H. Gao, *APL Energy*, 2024, **2**, 011503.

14 A. Dan, H. C. Barshilia, K. Chattopadhyay and B. Basu, *Renewable Sustainable Energy Rev.*, 2017, **79**, 1050–1077.

15 A. Rodríguez-Palomo, E. Céspedes, D. Hernández-Pinilla and C. Prieto, *Sol. Energy Mater. Sol. Cells*, 2018, **174**, 50–55.

16 D. Hernández-Pinilla, A. Rodríguez-Palomo, L. Álvarez-Fraga, E. Céspedes, J. E. Prieto, A. Muñoz-Martín and C. Prieto, *Sol. Energy Mater. Sol. Cells*, 2016, **152**, 141–146.

17 S. Huang, J. Zhang, H. Fu, Y. Xiong, S. Ma, X. Xiang, B. Xu, W. Lu, Y. Zhang, W. J. Weber and S. Zhao, *Prog. Mater. Sci.*, 2024, **143**, 101250.

18 C. Oses, C. Toher and S. Curtarolo, *Nat. Rev. Mater.*, 2020, **5**, 295–309.

19 W. Yang, J. Shen, Z. Wang, G. Ma, P. Ke and A. Wang, *J. Mater. Sci. Technol.*, 2025, **208**, 78–91.

20 H.-X. Guo, W.-M. Wang, C.-Y. He, B.-H. Liu, D.-M. Yu, G. Liu and X.-H. Gao, *ACS Appl. Mater. Interfaces*, 2022, **14**, 1950–1960.

21 C.-Y. He, P. Zhao, X.-H. Gao, G. Liu and P.-Q. La, *Mater. Today Phys.*, 2022, **27**, 100836.

22 L. Noč and I. Jerman, *Sol. Energy Mater. Sol. Cells*, 2022, **238**, 111625.

23 C.-Y. He, X.-H. Gao, D.-M. Yu, S.-S. Zhao, H.-X. Guo and G. Liu, *J. Mater. Chem. A*, 2021, **9**, 21270–21280.

24 P. Zhao, M. Dong, X. Liu, Y.-F. Wang, W.-M. Wang, B.-H. Liu, Z.-W. Lu, C.-Y. He and X.-H. Gao, *Adv. Funct. Mater.*, 2024, **34**, 2411316.

25 S. Akrami, P. Edalati, M. Fuji and K. Edalati, *Mater. Sci. Eng., R*, 2021, **146**, 100644.

26 L. Fei, Y. Yin, M. Yang, S. Zhang and C. Wang, *Energy Storage Mater.*, 2021, **42**, 636–644.

27 L. Xing, Y. Ha, R. Wang and Z. Li, *Sol. Energy*, 2023, **262**, 111858.

28 V. Verma, C. H. Belcher, D. Apelian and E. J. Lavernia, *Prog. Mater. Sci.*, 2024, **142**, 101245.

29 A. Ten, V. Lomonosov, C. Boukouvala and E. Ringe, *ACS Nano*, 2024, **18**, 18785–18799.

30 P. Das, S. Rudra, D. Rao, S. Banerjee, A. Indiradevi, M. Garbrecht, A. Boltasseva, I. V. Bondarev, V. M. Shalaev and B. Saha, *Sci. Adv.*, 2024, **10**, 2596.

31 R. A. Karaballi, G. Humagain, B. R. A. Fleischman and M. Dasog, *Angew. Chem., Int. Ed.*, 2019, **58**, 3147–3150.

32 Q. Wang, C. R. Bowen and V. K. Valev, *Adv. Funct. Mater.*, 2024, **34**, 2312245.

33 W.-T. Zhang, X.-Q. Wang, F.-Q. Zhang, X.-Y. Cui, B.-B. Fan, J.-M. Guo, Z.-M. Guo, R. Huang, W. Huang, X.-B. Li, M.-R. Li, Y. Ma, Z.-H. Shen, Y.-G. Sun, D.-Z. Wang, F.-Y. Wang, L.-Q. Wang, N. Wang, T.-L. Wang, W. Wang,
X.-Y. Wang, Y.-H. Wang, F.-J. Yu, Y.-Z. Yin, L.-K. Zhang, Y. Zhang, J.-Y. Zhang, Q. Zhao, Y.-P. Zhao, X.-D. Zhu, Y. Sohail, Y.-N. Chen, T. Feng, Q.-L. Gao, H.-Y. He, Y.-J. Huang, Z.-B. Jiao, H. Ji, Y. Jiang, Q. Li, X.-M. Li, W.-B. Liao, H.-J. Lin, H. Liu, Q. Liu, Q.-F. Liu, W.-D. Liu, X.-J. Liu, Y. Lu, Y.-P. Lu, W. Ma, X.-F. Miao, J. Pan, Q. Wang, H.-H. Wu, Y. Wu, T. Yang, W.-M. Yang, Q. Yu, J.-Y. Zhang, Z.-G. Chen, L. Mao, Y. Ren, B.-L. Shen, X.-L. Wang, Z. Jia, H. Zhu, Z.-D. Wu and S. Lan, *Rare Metals*, 2024, **43**, 4639–4776.

34 A. Calzolari, C. Oses, C. Toher, M. Esters, X. Campilongo, S. P. Stepanoff, D. E. Wolfe and S. Curtarolo, *Nat. Commun.*, 2022, **13**, 5993.

35 T. Ying, T. Yu, Y. Qi, X. Chen and H. Hosono, *Adv. Sci.*, 2022, **9**, 2203219.

36 D. N. Basov, M. M. Fogler and F. J. García de Abajo, *Science*, 2016, **354**, 1992.

37 C. Wang, Y. Hou, J. Cheng, M.-J. Lin and X. Wang, *Appl. Catal., B*, 2021, **294**, 120259.

38 J. Augustynski, K. Bienkowski and R. Solarska, *Coord. Chem. Rev.*, 2016, **325**, 116–124.

39 K. Li, L. Sun, W. Bai, N. Ma, C. Zhao, J. Zhao, C. Xiao and Y. Xie, *J. Am. Chem. Soc.*, 2024, **146**, 14318–14327.

40 Y. Liu, H. Xie, Z. Li, Y. Zhang, C. D. Malliakas, M. Al Malki, S. Ribet, S. Hao, T. Pham, Y. Wang, X. Hu, R. dos Reis, G. J. Snyder, C. Uher, C. Wolverton, M. G. Kanatzidis and V. P. Dravid, *J. Am. Chem. Soc.*, 2023, **145**, 8677–8688.

41 B. Wang, Q. Wang, B. Sun, J. Mo, Y. Guo, X. Liang and B. Shen, *J. Mater. Sci. Technol.*, 2023, **149**, 31–41.

42 Y. Liu, Y. Fu, F. Gu, H. Yu, L. Zhuang and Y. Chu, *Adv. Sci.*, 2025, **12**, 2501157.

43 H. Wang, Q. He, X. Gao, Y. Shang, W. Zhu, W. Zhao, Z. Chen, H. Gong and Y. Yang, *Adv. Mater.*, 2024, **36**, 2305453.

44 Z. An, S. Mao, Y. Liu, L. Wang, H. Zhou, B. Gan, Z. Zhang and X. Han, *J. Mater. Sci. Technol.*, 2021, **79**, 109–117.

45 Y. Li, J. Li, Y. Cao, Y. Zhong, J. Zeng, W. Xie, C. Li and W. Huang, *Nano Energy*, 2025, **138**, 110902.

46 Y. Wan, Y. Cheng, Y. Chen, Z. Zhang, Y. Liu, H. Gong, B. Shen and X. Liang, *Engineering*, 2023, **30**, 110–120.

47 Y. Li, C. Zhang, S. Peng, J. Zheng, X. Cui, S. Zhang and D. Sun, *Ceram. Int.*, 2025, **51**, 12396–12407.

48 S. R. Turner, S. Pailhès, F. Bourdarot, J. Ollivier, Y. Sidis, J.-P. Castellan, J.-M. Zanotti, Q. Berrod, F. Porcher, A. Bosak, M. Feuerbacher, H. Schober, M. de Boissieu and V. M. Giordano, *Nat. Commun.*, 2022, **13**, 7509.

49 F. Körmann, Y. Ikeda, B. Grabowski and M. H. F. Sluiter, *npj Comput. Mater.*, 2017, **3**, 36.

50 P. L. Gentili and J.-C. Micheau, *J. Photochem. Photobiol., C*, 2020, **43**, 100321.

51 D. Chester, P. Bermel, J. D. Joannopoulos, M. Soljacic and I. Celanovic, *Opt. Express*, 2011, **19**, A245–A257.

52 X. Wang, X. Yu, S. Fu, E. Lee, K. Kekalo and J. Liu, *J. Appl. Phys.*, 2018, **123**, 033104.

53 Z. Qi-Chu, *J. Phys. D: Appl. Phys.*, 1999, **32**, 1938.

54 N. Selvakumar, S. B. Krupanidhi and H. C. Barshilia, *Adv. Mater.*, 2014, **26**, 2552–2557.

55 L. Rebouta, A. Pitães, M. Andritschky, P. Capela, M. F. Cerqueira, A. Matilainen and K. Pischow, *Surf. Coat. Technol.*, 2012, **211**, 41–44.

56 Y. Li, C. Lin, Z. Wu, Z. Chen, C. Chi, F. Cao, D. Mei, H. Yan, C. Y. Tso, C. Y. H. Chao and B. Huang, *Adv. Mater.*, 2021, **33**, 2005074.

57 Y. S. Kwon, Y. Li and B. Huang, *ES Mater. Manuf.*, 2023, **20**, 812.

58 J. Zhou, S. Zhang and J. Wang, *J. Energy Storage*, 2024, **104**, 114476.

59 H.-X. Guo, D.-M. Yu, C.-Y. He, X.-L. Qiu, S.-S. Zhao, G. Liu and X.-H. Gao, *Surf. Interfaces*, 2021, **24**, 101062.

60 N. Selvakumar and H. C. Barshilia, *Sol. Energy Mater. Sol. Cells*, 2012, **98**, 1–23.

61 C. Le Paven-Thivet, L. Le Gendre, J. Le Castrec, F. Cheviré, F. Tessier and J. Pinel, *Prog. Solid State Chem.*, 2007, **35**, 299–308.

62 C. Han, D. Chen, Y. Zhang, D. Xu, Y. Liu, E. S.-W. Kong and Y. Zhang, *Nano-Micro Lett.*, 2012, **4**, 40–44.

63 L. Sun, G. Yuan, L. Gao, J. Yang, M. Chhowalla, M. H. Gharahcheshmeh, K. K. Gleason, Y. S. Choi, B. H. Hong and Z. Liu, *Nat. Rev. Methods Primers*, 2021, **1**, 5.

64 J. A. Raiford, S. T. Oyakhire and S. F. Bent, *Energy Environ. Sci.*, 2020, **13**, 1997–2023.

65 R. Burns, D. Chiaro, H. Davison, C. J. Arendse, G. M. King and S. Guha, *Small*, 2025, **21**, 2406815.

66 E. Erben, R. Bertinger, A. Mühlratzer, B. Tihanyi and B. Cornils, *Sol. Energy Mater.*, 1985, **12**, 239–248.

67 A. Lalisse, G. Tessier, J. Plain and G. Baffou, *Sci. Rep.*, 2016, **6**, 38647.

68 T. K. Tsai, Y. H. Li and J. S. Fang, *Thin Solid Films*, 2016, **615**, 91–96.

69 D. Zhu and S. Zhao, *Sol. Energy Mater. Sol. Cells*, 2010, **94**, 1630–1635.

70 H.-X. Guo, C.-Y. He, X.-L. Qiu, Y.-Q. Shen, G. Liu and X.-H. Gao, *Sol. Energy Mater. Sol. Cells*, 2020, **209**, 110444.

71 C.-Y. He, X.-L. Qiu, D.-M. Yu, S.-S. Zhao, H.-X. Guo, G. Liu and X.-H. Gao, *J. Materiomics*, 2021, **7**, 460–469.

72 W.-J. Sheng, X. Yang, J. Zhu, C. Wang and Y. Zhang, *Rare Metals*, 2018, **37**, 682–689.

73 M. Kotilainen, M. Honkanen, K. Mizohata and P. Vuoristo, *Sol. Energy Mater. Sol. Cells*, 2016, **145**, 323–332.

74 X.-H. Gao, Z.-M. Guo, Q.-F. Geng, P.-J. Ma, A.-Q. Wang and G. Liu, *Sol. Energy Mater. Sol. Cells*, 2017, **163**, 91–97.

75 C.-Y. He, X.-H. Gao, D.-M. Yu, X.-L. Qiu, H.-X. Guo and G. Liu, *J. Mater. Chem. A*, 2021, **9**, 6413–6422.

76 H. C. Barshilia, N. Selvakumar, K. S. Rajam, D. V. Sridhara Rao, K. Muraleedharan and A. Biswas, *Appl. Phys. Lett.*, 2006, **89**, 191909.

77 H. C. Barshilia, N. Selvakumar, K. S. Rajam and A. Biswas, *Sol. Energy Mater. Sol. Cells*, 2008, **92**, 495–504.

78 A. Al-Rjoub, L. Rebouta, P. Costa and L. G. Vieira, *Sol. Energy Mater. Sol. Cells*, 2018, **186**, 300–308.

79 L. Rebouta, P. Capela, M. Andritschky, A. Matilainen, P. Santilli, K. Pischow and E. Alves, *Sol. Energy Mater. Sol. Cells*, 2012, **105**, 202–207.

80 H. C. Barshilia, K. Niranjan, G. Srinivas, S. John and N. T. Manikandanath, *Sol. Energy Mater. Sol. Cells*, 2022, **241**, 111746.

81 Y. Li, C. Lin, D. Zhou, Y. An, D. Li, C. Chi, H. Huang, S. Yang, C. Y. Tso, C. Y. H. Chao and B. Huang, *Nano Energy*, 2019, **64**, 103947.

82 A. Dan, J. Jyothi, K. Chattopadhyay, H. C. Barshilia and B. Basu, *Sol. Energy Mater. Sol. Cells*, 2016, **157**, 716–726.

83 N. Selvakumar, K. Prajith, A. Biswas and H. C. Barshilia, *Sol. Energy Mater. Sol. Cells*, 2015, **140**, 328–334.

84 N. Selvakumar, N. T. Manikandanath, A. Biswas and H. C. Barshilia, *Sol. Energy Mater. Sol. Cells*, 2012, **102**, 86–92.

85 Y. Wu, C. Wang, Y. Sun, Y. Ning, Y. Liu, Y. Xue, W. Wang, S. Zhao, E. Tomasella and A. Bousquet, *Sol. Energy*, 2015, **119**, 18–28.

86 C.-Y. He, P. Zhao, H. Zhang, K. Chen, B.-H. Liu, Z.-W. Lu, Y. Li, P.-Q. La, G. Liu and X.-H. Gao, *Adv. Sci.*, 2023, **10**, 2204817.

87 C.-Y. He, Z. Li, P. Zhao, H.-C. Jiang, Z.-H. Zhou, R.-T. Gao, P.-Q. La, L. Wang and X.-H. Gao, *EcoEnergy*, 2025, **3**, 156–169.

88 A. G. Wattoo, R. Bagheri, X. Ding, B. Zheng, J. Liu, C. Xu, L. Yang and Z. Song, *J. Mater. Chem. C*, 2018, **6**, 8646–8662.

89 P. Song, C. Wang, J. Ren, Y. Sun, Y. Zhang, A. Bousquet, T. Sauvage and E. Tomasella, *Int. J. Miner., Metall. Mater.*, 2020, **27**, 1371–1378.

90 Y. Li, W. Ma, Y. S. Kwon, W. Li, S. Yao and B. Huang, *Adv. Funct. Mater.*, 2022, **32**, 2113297.

91 Y. Fei, Q. Wang, F. Wang, G. Zhang, M. Hu, T. Ding, T. Zhao and X. Xiao, *InfoMat*, 2025, **7**, e12654.

92 X.-L. Qiu, C.-Y. He, P. Zhao, B.-H. Liu, H.-X. Guo, G. Liu and X.-H. Gao, *Mater. Today Phys.*, 2022, **24**, 100690.

93 Y. Li, C. Xiong, H. Huang, X. Peng, D. Mei, M. Li, G. Liu, M. Wu, T. Zhao and B. Huang, *Adv. Mater.*, 2021, **33**, 2103054.

94 K. Zhang, L. Hao, M. Du, J. Mi, J.-N. Wang and J.-p. Meng, *Renewable Sustainable Energy Rev.*, 2017, **67**, 1282–1299.

95 J. Moon, D. Lu, B. VanSaders, T. K. Kim, S. D. Kong, S. Jin, R. Chen and Z. Liu, *Nano Energy*, 2014, **8**, 238–246.

96 J. Chen, C. Guo, J. Chen, J. He, Y. Ren and L. Hu, *Mater. Lett.*, 2014, **133**, 71–74.

97 J. Geng, L. Shi, J. Ni, Q. Jia, W. Yan and M. Qiu, *PhotoniX*, 2022, **3**, 14.

98 J. Zhang, X. Li, M. Zhong, Z. Zhang, M. Jia, J. Li, X. Gao, L. Chen, Q. Li, W. Zhang and D. Xu, *Small*, 2022, **18**, 2201716.

99 Y. Chu, B. Cui and F. Monteverde, *J. Materiomics.*, 2025, **11**, 100966.

100 Y. Li, Z. Luo, S. E. Skrabalak and Y. Xiong, *ACS Mater. Lett.*, 2024, **6**, 2696–2697.

101 B. Ren, R.-f. Zhao, G.-p. Zhang, Z.-x. Liu, B. Cai and A.-y. Jiang, *Ceram. Int.*, 2022, **48**, 16901–16911.

102 R. Escobar-Galindo, I. Heras, E. Guillén, F. Lungwitz, G. Rincón-Llorente, F. Munnik, I. Azkona and M. Krause, *Sol. Energy Mater. Sol. Cells*, 2024, **271**, 112865.

103 A. Dan, A. Biswas, P. Sarkar, S. Kashyap, K. Chattopadhyay, H. C. Barshilia and B. Basu, *Sol. Energy Mater. Sol. Cells*, 2018, **176**, 157–166.

104 Y. Wang, Y. Tang, W. Wan and X. Zhang, *J. Mater. Eng. Perform.*, 2020, **29**, 6412–6416.

105 P. Song, Y. Wu, L. Wang, Y. Sun, Y. Ning, Y. Zhang, B. Dai, E. Tomasella, A. Bousquet and C. Wang, *Sol. Energy Mater. Sol. Cells*, 2017, **171**, 253–257.

106 Q. Y. Li, S. J. Dong, Q. Cao, W. P. Ye, D. Q. Gong and X. D. Cheng, *Appl. Surf. Sci.*, 2019, **498**, 143886.

107 N. Selvakumar, S. Santhoshkumar, S. Basu, A. Biswas and H. C. Barshilia, *Sol. Energy Mater. Sol. Cells*, 2013, **109**, 97–103.

108 X. Wang, X. Yuan, D. Gong, X. Cheng and K. Li, *J. Mater. Res. Technol.*, 2021, **15**, 6162–6174.

109 Y. H. Liang and E. Towe, *Appl. Phys. Rev.*, 2018, **5**, 011107.

110 C. Zou, W. Xie and L. Shao, *Sol. Energy Mater. Sol. Cells*, 2016, **153**, 9–17.

111 H. Wen, W. Wang, W. Wang, J. Su, T. Lei and C. Wang, *Sol. Energy Mater. Sol. Cells*, 2019, **202**, 110152.

112 Y. Guo, K. Tsuda, S. Hosseini, Y. Murakami, A. Tricoli, J. Coventry, W. Lipiński and J. F. Torres, *Nat. Commun.*, 2024, **15**, 384.

113 R. A. Karaballi, Y. E. Monfared and M. Dasog, *Chem.–Eur. J.*, 2020, **26**, 8499–8505.

114 M. Kumar, N. Umezawa, S. Ishii and T. Nagao, *ACS Photonics*, 2016, **3**, 43–50.

115 U. Guler, V. M. Shalaev and A. Boltasseva, *Mater. Today*, 2015, **18**, 227–237.

116 P. Patsalas, N. Kalfagiannis, S. Kassavetis, G. Abadias, D. V. Bellas, C. Lekka and E. Lidorikis, *Mater. Sci. Eng., R*, 2018, **123**, 1–55.

117 M. B. Cortie, J. Giddings and A. Dowd, *Nanotechnology*, 2010, **21**, 115201.

118 H. Reddy, U. Guler, Z. Kudyshev, A. V. Kildishev, V. M. Shalaev and A. Boltasseva, *ACS Photonics*, 2017, **4**, 1413–1420.

119 F. Cao, L. Tang, Y. Li, A. P. Litvinchuk, J. Bao and Z. Ren, *Sol. Energy Mater. Sol. Cells*, 2017, **160**, 12–17.

120 D. Kraemer, B. Poudel, H.-P. Feng, J. C. Caylor, B. Yu, X. Yan, Y. Ma, X. Wang, D. Wang, A. Muto, K. McEnaney, M. Chiesa, Z. Ren and G. Chen, *Nat. Mater.*, 2011, **10**, 532–538.

121 D. Jiang, Z. Fan, M. Dong, Y. Shang, X. Liu, G. Chen and S. Li, *Appl. Therm. Eng.*, 2018, **141**, 828–834.

122 B. S. Almutairi, M. Alomar, N. Arshad, A. A. Hendi, M. S. Irshad and I. Ahmed, *Energy Technol.*, 2024, **12**, 2301026.

123 X. Liu, P. Zhao, C.-Y. He, W.-M. Wang, B.-H. Liu, Z.-W. Lu, Y.-F. Wang, H.-X. Guo, G. Liu and X.-H. Gao, *ACS Appl. Mater. Interfaces*, 2022, **14**, 50180–50189.

124 C. Chang, P. Tao, B. Fu, J. Xu, C. Song, J. Wu, W. Shang and T. Deng, *ACS Omega*, 2019, **4**, 3546–3555.

125 Y. Bian, K. Tang, L. Tian, L. Zhao, S. Zhu, H. Lu, Y. Yang, J. Ye and S. Gu, *ACS Appl. Mater. Interfaces*, 2021, **13**, 4935–4942.

126 A. K. Menon, I. Haechler, S. Kaur, S. Lubner and R. S. Prasher, *Nat Sustainability*, 2020, **3**, 144–151.

127 Y. Zhang, Y. Li, K. Li, Y. S. Kwon, T. Tennakoon, C. Wang, K. C. Chan, S.-C. Fu, B. Huang and C. Y. H. Chao, *Nano Energy*, 2022, **95**, 106996.

128 S. Dash, J. de Ruiter and K. K. Varanasi, *Sci. Adv.*, 4, eaat0127.

129 W. Ma, Y. Li, C. Y. H. Chao, C. Y. Tso, B. Huang, W. Li and S. Yao, *Cell Rep. Phys. Sci.*, 2021, **2**, 100384.

130 B. Liu, C. Wang, S. Bazri, I. A. Badruddin, Y. Orooji, S. Saeidi, S. Wongwises and O. Mahian, *Powder Technol.*, 2021, **377**, 939–957.

131 G. K. Manikandan, S. Iniyan and R. Goic, *Appl. Energy*, 2019, **235**, 1524–1540.

132 H. Ait-Sadi, D. Bekhiti, L. Hemmouche, R. Zellagui and A. Halimi, *Renewable Sustainable Energy Rev.*, 2025, **211**, 115270.

133 F. Cao, K. McEnaney, G. Chen and Z. Ren, *Energy Environ. Sci.*, 2014, **7**, 1615–1627.

134 L. Hao, M. Du, X. Liu, S. Wang, L. Jiang, F. Lü, Z. Li and J. Mi, *Sci. China: Technol. Sci.*, 2010, **53**, 1507–1512.

135 Q. Tang, B. Jiang, K. Wang, W. Wang, B. Jia, T. Ding, Z. Huang, Y. Lin and J. He, *Joule*, 2024, **8**, 1641–1666.

136 E. Toberer, *Nat. Energy*, 2016, **1**, 16172.

137 A. A. Candadai, V. P. Kumar and H. C. Barshilia, *Sol. Energy Mater. Sol. Cells*, 2016, **145**, 333–341.

138 D. Kraemer, Q. Jie, K. McEnaney, F. Cao, W. Liu, L. A. Weinstein, J. Loomis, Z. Ren and G. Chen, *Nat. Energy*, 2016, **1**, 16153.

139 P. Cheruvu, K. V. Praveen and H. C. Barshilia, *Int. J. Sustain. Energy*, 2018, **37**, 782–798.

140 D. Wei, C. Wang, J. Zhang, H. Zhao, Y. Asakura, M. Eguchi, X. Xu and Y. Yamauchi, *Adv. Mater.*, 2023, **35**, 2212100.

141 J. Zhang, C. Wang, J. Shi, D. Wei, H. Zhao and C. Ma, *Adv. Energy Sustainability Res.*, 2022, **3**, 2100195.

142 Y. Guo, X. Zhao, F. Zhao, Z. Jiao, X. Zhou and G. Yu, *Energy Environ. Sci.*, 2020, **13**, 2087–2095.

143 G. Ni, G. Li, S. V. Boriskina, H. Li, W. Yang, T. Zhang and G. Chen, *Nat. Energy*, 2016, **1**, 16126.

144 W. Wang, Y. Shi, C. Zhang, S. Hong, L. Shi, J. Chang, R. Li, Y. Jin, C. Ong, S. Zhuo and P. Wang, *Nat. Commun.*, 2019, **10**, 3012.

145 L. Tang, B. Lyu, D. Gao, Z. Jia, Y. Fu and J. Ma, *Small*, 2024, **20**, 2308194.

146 J. Wang, M. Shen, Z. Liu and W. Wang, *Nano Energy*, 2022, **97**, 107177.

147 V. Daniliuk, Y. Xu, R. Liu, T. He and X. Wang, *Renewable Energy*, 2020, **145**, 2005–2018.

148 L. Zhang, Y. Feng, X. Cao, Y. Dong, W. Liu, B. Li, J. Li and C. Hao, *Adv. Sci.*, 2025, **12**, 2502945.

149 X.-M. Xie, J.-F. Su, Y.-D. Guo and L.-Q. Wang, *J. Clean. Prod.*, 2020, **274**, 122947.

150 H. Ma, H. Yu, C. Li, Y. Tan, W. Cao and B. Da, *Constr. Build. Mater.*, 2018, **187**, 197–204.

151 H.-C. Dan, J.-W. Tan, Y.-F. Du and J.-M. Cai, *Cold Reg. Sci. Technol.*, 2020, **169**, 102917.

152 T. N. H. Lo, H. S. Hwang, J. Lee and I. Park, *Prog. Org. Coat.*, 2020, **148**, 105853.

153 C. Hu, K. Guo, Y. Li, Z. Gu, J. Quan, S. Zhang and W. Zheng, *Thin Solid Films*, 2019, **688**, 137339.

154 M. Okada, A. Hosokawa, R. Tanaka and T. Ueda, *Int. J. Mach. Tools Manuf.*, 2011, **51**, 127–132.

155 S. Yang, J. Liu, M. J. Hoque, A. Huang, Y. Chen, W. Yang, J. Feng and N. Miljkovic, *Adv. Mater.*, 2025, **37**, 2415237.

156 Y. Liu, Y. Wu, Y. Liu, R. Xu, S. Liu and F. Zhou, *ACS Appl. Mater. Interfaces*, 2020, **12**, 46981–46990.

157 T. Hao, D. Wang, X. Chen, A. Jazzar, P. Shi, C. Li, H. Wang, X. He and Z. He, *Appl. Phys. Rev.*, 2023, **10**, 021317.

158 X. Huang, N. Tepylo, V. Pommier-Budinger, M. Budinger, E. Bonaccurso, P. Villedieu and L. Bennani, *Prog. Aeronaut. Sci.*, 2019, **105**, 74–97.

159 C.-Y. He, P. Zhao, B.-H. Liu, Z.-W. Lu, X.-H. Gao, G. Liu and P.-Q. La, *ACS Appl. Energy Mater.*, 2022, **5**, 11517–11525.

160 C.-Y. He, X.-H. Gao, D.-M. Yu, H.-X. Guo, S.-S. Zhao and G. Liu, *ACS Appl. Mater. Interfaces*, 2021, **13**, 16987–16996.

161 C.-Y. He, X.-H. Gao, X.-L. Qiu, D.-M. Yu, H.-X. Guo and G. Liu, *Sol. RRL*, 2021, **5**, 2000790.